J. Coat. Technol. Res.
https://doi.org/10.1007/s11998-025-01190-9

Degradation of structural aircraft coatings in cyclic salt spray testing, outdoor exposure, and in-service environments

A. J. Cornet, A. M. Homborg, L. 't Hoen-Velterop, J. M. C. Mol

Received: 17 April 2025 / Revised: 1 July 2025 / Accepted: 23 July 2025

Abstract Developing accelerated exposure tests that accurately predict the in-service performance of structural aircraft coatings remains challenging, largely due to the complexity of simulating real-world environmental conditions without altering key degradation mechanisms. This study evaluated four different coating systems under various accelerated exposure tests and compared their degradation behavior to in-service performance. Coating degradation was characterized using electrochemical impedance spectroscopy, scanning electron microscopy, and attenuated total reflectance Fourier transform infrared spectroscopy. Under in-service conditions, failure was primarily driven by the leaching of corrosion inhibitors, while the polymer matrix degraded predominantly through hydrolysis and thermo-oxidation. In contrast, during outdoor- or cyclic salt spray exposure, inhibitor leaching remained a key contributor to coating degradation although polymer degradation was mainly caused by ultraviolet radiation or hydrolysis. These findings emphasize the challenge of replicating real-world degradation in laboratory settings. Additionally, anodized oxide layers containing polymers within their pores played a critical role in maintaining protection during early coating failure. Chromate-based systems restored barrier properties, likely through chromate adsorption on hydrolyzed products within the oxide pores. In comparison, praseodymium-based systems failed to restore protection, while lithium-based systems sustained protection through an intact polymer.

Keywords Coatings, Outdoor exposure, Cyclic salt spray test, In-service ageing, Corrosion

A. J. Cornet (✉), A. M. Homborg, J. M. C. Mol
Department of Materials Science and Engineering, Delft University of Technology, Mekelweg 2, 2628 CD Delft, The Netherlands
e-mail: A.J.Cornet@TUDelft.nl

A. J. Cornet
Royal Netherlands Air Force, Kooiweg 40, 4631 SZ Hoogerheide, The Netherlands

A. M. Homborg
Netherlands Defence Academy, Het Nieuwe Diep 8, 1781 AC Den Helder, The Netherlands

L. 't Hoen-Velterop
National Aerospace Laboratory, Voorsterweg 31, 8316 PR Marknesse, The Netherlands

Introduction

Aluminium alloy components used in the aerospace industry require robust protection against corrosion and environmental degradation. This is typically achieved through a multilayered coating system.[1–3] A coating system typically consists of a pretreatment layer, such as an anodised oxide layer or a chemical conversion coating, with on top a primer containing active corrosion inhibitors.[2–5] The organic coatings applied for structural applications are an essential part of the overall coating system. In certain cases, an additional topcoat may be applied, although its use is generally restricted to areas exposed to severe corrosive environments. The primary function of the coating system is to act as a barrier against moisture and electrolytes, while simultaneously providing active corrosion protection by the release of embedded inhibitors to protect the substrate at damaged areas.[3]

Currently, chromate-based inhibitors dominate the aerospace industry due to their exceptional performance in active corrosion protection.[3, 6, 7] However, chromates are highly toxic and carcinogenic, creating an urgent need for safer, more environmentally friendly alternatives.[8, 9] Significant research has been conducted to develop chromate-free coatings, includ-

Published online: 26 January 2026

ing formulations that incorporate rare earth-based compounds or lithium salts as alternative corrosion inhibitors.[6, 10–15] Despite these advances, achieving the protective performance of chromate-based coating systems by alternative coating systems remains challenging.[6, 16]

To assess the performance of novel coatings, accelerated testing methods such as salt spray and outdoor exposure tests are widely used.[17–20] However, these standardized tests often fail to replicate the complex degradation mechanisms that occur under real-world service conditions.[18, 19, 21, 22] One of the key challenges is accelerating corrosion without introducing artificial factors that do not accurately reflect actual operational environments.[18, 19, 22]

Extensive research has been conducted to enhance the reliability of corrosion testing.[17, 19, 20, 23] This has led to the improvement of the widely used neutral salt spray test (ASTM B117, ISO 9227) into the more advanced cyclic corrosion tests, such as ASTM G85, SAE J2334, VDA 233-102, and VCS 1027, 149.[17, 19, 20, 23] Although these cyclic tests are intended to provide a better correlation between laboratory results and real-world performance, establishing a direct relationship remains difficult. Notably, studies have shown that variations in time of wetness lead to different corrosion phenomena; extended wet phases tend to promote blistering, whereas dry or humid cycles are more likely to induce filiform corrosion.[20,23] As a result, defining reliable qualification criteria for aerospace coatings continues to be a challenge.[18,19]

Moreover, the aerospace industry encompasses a broad range of coating applications, each exposed to unique environmental conditions, while most cyclic corrosion tests are designed to simulate natural weathering making these suitable for evaluating exterior coating systems.[24] However, these tests do not adequately replicate the degradation conditions experienced by structural coating systems. Except for a number of specific cases, corrosion protection in structural applications often relies on primer-only systems, which are not designed to withstand UV radiation and prolonged electrolyte exposure. Instead, structural primers face unique challenges, such as crevice corrosion, exposure to aircraft fluids, and application on complex geometries, which are not effectively captured by standardized cyclic salt spray tests (CSST) protocols. Although factors like humidity and temperature fluctuations affect both exterior and structural parts, the resulting corrosion and degradation mechanisms can differ significantly.

As structural primers are being reformulated to eliminate chromate-based inhibitors, there is a pressing need to develop test methods that accurately reflect their specific exposure conditions. Without corrosion tests tailored to structural aerospace applications, it remains difficult to assess the long-term in-service coating performance of newly formulated chromate-free coating systems. Developing more accurate and representative testing methods is therefore essential. This will not only improve performance predictions, but also accelerate the adoption of safer and more sustainable coating solutions.

To enhance the reliability of these testing methods, a deeper understanding of how environmental factors affect the degradation of coatings and corrosion in structural applications is needed. Therefore, this study investigates the degradation mechanisms of structural aerospace coating systems under (i) accelerated conditions, such as cyclic salt spray testing, (ii) natural weathering through outdoor exposure, and (iii) real-world conditions during flight testing, where coatings are exposed in structural environments. The research focuses on two primary aspects of coating degradation: the degradation of the polymer matrix and the leaching behavior of corrosion inhibitors.

To characterize these processes, a multidisciplinary approach was employed. Electrochemical impedance spectroscopy (EIS) was used to monitor changes in the electrochemical properties of the coating systems during electrolyte immersion, providing insights into their protective behavior over time. Scanning electron microscopy (SEM) was applied to examine morphological changes in the coating structure after exposure to various environmental conditions. Additionally, attenuated total reflectance Fourier transform infrared spectroscopy (ATR-FTIR) was used to investigate chemical changes in the polymer matrix induced by environmental stressors.

By integrating these analytical techniques, this study provides a comprehensive understanding of the fundamental degradation mechanisms affecting the performance of structural aerospace coatings. The findings contribute to the development of more reliable testing methodologies and offer valuable insights for designing durable, effective chromate-free protective coatings for structural aerospace applications.

Materials and methods

Test samples

In earlier work, the focus was on corrosion-induced degradation of the metal substrate and the protective effects of inhibitors at specific defect sites under various exposure conditions. Full details of the experimental methods are available in the accompanying publication.[22] The present study shifts attention to the degradation of the same samples specifically evaluating the four visually intact coating systems: two chromate-containing systems and two alternatives based on praseodymium and lithium inhibitors. The chromate-

containing coatings were selected to assess whether accelerated test methods can reliably predict long-term in-service performance. Notably, the performance of the chromate−1 system has already been evaluated on aircraft components after more than 35 years of service.[25, 26] Meanwhile, the chromate−2 system is accredited for the same application, making it a strong benchmark for determining whether other coating systems can achieve comparable long-term performance based on accelerated testing. To identify key degradation factors, the coatings were exposed to various environmental conditions, including:

i. Immersion testing (as a reference)
ii. Two-year outdoor exposure
iii. 1000-h CSST
iv. 2.5 years of in-service exposure (flight testing)

All coatings were applied to anodized aluminium alloy (AA)2024-T62 substrates, featuring anodized oxide layers of approximately 2 μm thick. The dry-film thickness of each coating was approximately 25 μm. The nominal chemical composition of the AA2024-T62 alloy is as follows: Cu 4 wt%; Mg 1.5 wt%; Mn 0.6 wt%; Si 0.5 wt%; Fe 0.5 wt%; Zn 0.25 wt%; Ti 0.15 wt%; and Cr 0.10 wt%; with the balance Al. Table 1 provides an overview of the coating systems evaluated in this study.

As noted in Table 1, the chromate−1, chromate−2, and praseodymium coating systems are based on a polyamide epoxy resin, in compliance with MIL-PRF-23377, the military standard that defines performance requirements for primer coatings. By contrast, the manufacturer of the lithium-based coating selected a polyurethane resin, which offers greater resistance to moisture ingress and polymer chain scission. This formulation was intended to address the challenge of developing a robust alternative to chromate-containing systems. However, while reduced moisture permeability improves barrier performance, it can also hinder the timely release of corrosion inhibitors, which rely on moisture to dissolve and activate. The lithium-based system was therefore in this study specifically selected to assess the effectiveness of active corrosion inhibition in a low-permeability coating matrix.

Exposure environments

Environmental conditions during these tests have been described in detail in a separate study[22]; a summarized overview is provided in Table 2.

Immersion testing

The immersion test served as a reference to support interpretation of the results from other exposure conditions, particularly by correlating EIS data with physical degradation features observed in SEM cross sections, as demonstrated in a previous study.[26] In this test, 10 cm^2 of a coated, anodized aluminium substrate was exposed to a 0.1 M NaCl solution within an EIS cell. This salinity was intentionally selected to provide stable and reliable EIS measurements, allowing for the gradual monitoring of coating degradation over time. Further details on EIS and SEM analysis are provided in ''Electrochemical impedance spectroscopy (EIS)'' and ''Scanning electron microscopy (SEM)'' sections, respectively.

Outdoor exposure

Outdoor exposure testing was conducted because it is widely recognized as a benchmark for evaluating the in-service performance of protective coatings.[17, 19, 23] Although structural coatings on aircraft are typically shielded from direct UV radiation and rainfall during service, exposing these to such conditions provides valuable insights; outdoor exposure can reveal severe degradation mechanisms and failure modes that may not emerge during shorter in-service exposure periods or through accelerated laboratory testing such as CSST. This helps in identifying potential long-term degradation pathways.

Furthermore, the test panels included regions, such as the back sides, that were naturally shielded from direct UV and rain. These areas can serve as references for in-service degradation. At the same time, side-by-side comparisons between indirectly and fully exposed

Table 1: Coating systems under evaluation

Coating system	Substrate material	Pre-treatment	Primer
Chromate−1	AA2024-T62	Chromic acid anodized MIL-A-8625, Type I	$SrCrO_4$ epoxy-polyamide primer, manufacturer 1
Chromate−2	AA2024-T62	Chromic acid anodized MIL-A-8625, Type I	$SrCrO_4$ epoxy-polyamide primer, manufacturer 2
Praseodymium	AA2024-T62	Thin film sulfuric acid anodized MIL-A-8625, Type IIB	Praseodymium epoxy-polyamide primer
Lithium	AA2024-T62	Thin film sulfuric acid anodized MIL-A-8625, Type IIB	Lithium polyurethane primer

Table 2: Summary of corrosion-related environmental conditions during different exposure tests

	Outdoor exposure (2 y)	Cyclic salt spray test (1000 h)	Flight test (2.5 y)
Avg. temperature during TOW (°C)	10 ± 14	40 ± 3	10 ± 9
Total TOW (h)	9651	500	3904
RH-cycles	813	500	319

surfaces are still possible, offering a more nuanced understanding of how different environmental stressors affect coating degradation and how these findings relate to in-service conditions. In addition, the performance of fully exposed surfaces under outdoor conditions correlates more closely with samples tested in CSST (except for the UV exposure), further justifying the inclusion of outdoor exposure testing as a complementary reference for evaluating coating durability.

Outdoor exposure tests were conducted at Naval Air Station De Kooy in Den Helder, the Netherlands. The panels were mounted on an outdoor exposure rack from 18 March 2022 to 18 March 2024. The rack was attached to the air traffic control tower, facing south southwest, at an elevation of 14 m as shown in Fig. 1. The panels were mounted vertically (90° relative to the horizon).

The panels were visually inspected every three months. EIS measurements were performed on-site during these inspections. The methodology for EIS measurements is further detailed in ''Electrochemical impedance spectroscopy (EIS)'' section.

Cyclic salt spray test (CSST)

To better replicate in-service atmospheric corrosion behavior, a customized cyclic corrosion protocol based on the methodology as proposed by Dante et al.[27] was used in this study. This protocol was developed through detailed investigations of environmental parameters such as relative humidity cycling, salt chemistry, and time of wetness. Relative to the standard CSST, this protocol has been reported to produce corrosion mechanisms that more closely reflect those observed under actual service conditions.

The CSST was conducted using an Ascott CC450iP salt spray chamber. The test panels were positioned at a 7° vertical angle within the chamber and subjected to 500 cycles under the following conditions:

I. 1-h high humidity period:

a. 15 min of salt spray using ASTM-D1193 Type IV artificial seawater solution, acidified to pH 3 with HCl;
b. 45 min of high humidity exposure (> 80% relative humidity, RH).

II. 1-hour dry-off period:

a. Ramp rate: RH reduced from 80 to 30% within 25 min;
b. RH reduced to below 30% for at least 35 min.

The cabinet conditions during the test were maintained as follows:

- Atomized nozzle pressure: 10–25 PSI;
- Bubble tower temperature: 47°C;
- Salt spray chamber temperature: 40 ± 3°C;
- Fog collection rate: 1.0–2.0 mL/h of continuous spray per 80 cm^2 (measured over at least 16 h with a minimum of two collectors).

Flight testing

Flight testing was conducted on three identical aircraft, all operating from the same airbase under comparable service conditions over a period of 2.5 years. During this time, each aircraft accumulated an average of approximately 275 flight hours. This test included the evaluation of the chromate−2, praseodymium, and lithium coating systems. Chromate−1 was excluded from the evaluation as it was unavailable at the time of the preparation of the flight test panels.

Test panels were installed on the aircraft in standardized configurations and inspected every 3 months, with on-site EIS measurements conducted during each inspection. All panels were identical in design and construction, however mounted at different angles: the praseodymium and lithium panels were installed vertically (approximately 90° relative to the horizon), whereas the chromate−2 panel was mounted at a 30° angle (relative to the horizon).

A schematic example of an in-service test panel configuration is shown in Fig. 2.

Evaluation methods

Electrochemical impedance spectroscopy (EIS)

EIS measurements were performed at regular intervals throughout the exposure period using a Biologic VSP-300 potentiostat. The measurements were conducted over a frequency range of 10^{-2} to 10^{5} Hz, with seven points per decade utilizing a two-electrode setup. A

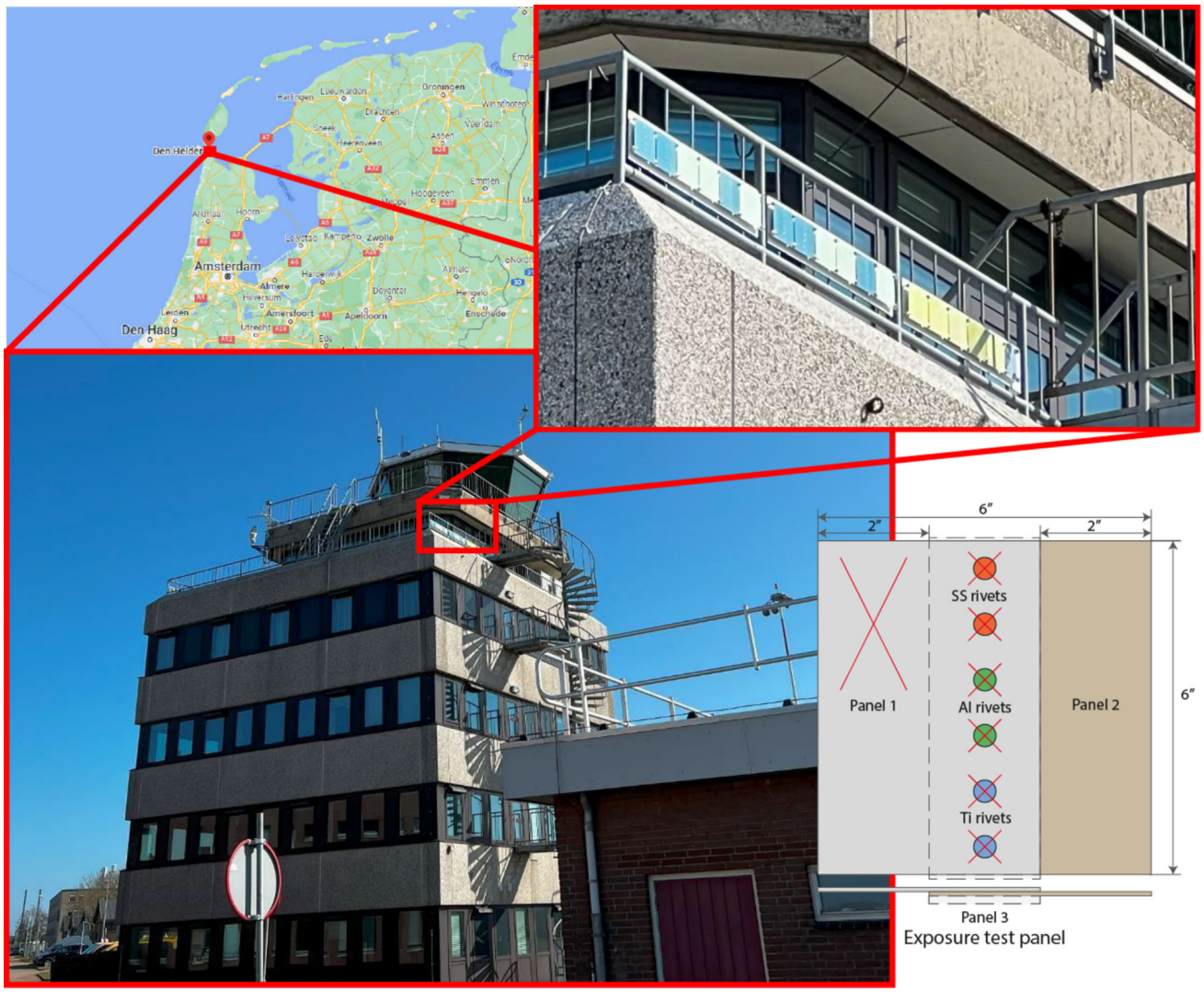

Fig. 1: Exposure panel mounted on the air traffic control tower at Naval Air Station De Kooy in Den Helder, The Netherlands, during outdoor exposure testing

sinusoidal amplitude of 150 mV was selected to minimize interference effects during field measurements.[28]

For laboratory measurements, experiments were carried out inside a Faraday cage to minimize external electromagnetic interference. The coated sample served as the working electrode, while a carbon rod functioned as the counter electrode. To ensure precise electrolyte exposure, custom-designed cells were used to expose exactly 10 cm^2 of the coated anodized aluminium substrate to 35 mL of 0.1 M sodium chloride (NaCl) solution. These cells were securely mounted onto the samples using Dowsil 3145 RTV sealant to create a watertight seal.

For field measurements, coatings were pre-wetted with saturated pads containing 0.1 M NaCl solution for exactly 2 h before testing, ensuring consistent electrochemical conditions. Circular pre-wetting pads (36 mm in diameter, approximately 10 cm^2) were made from 3 M Scotch-Brite 98 material. Axion sticker electrodes (40 mm × 40 mm) were used for the EIS measurements, with one electrode serving as the working electrode and the other functioning as both the counter and reference electrode. To mitigate external interference during in-field aircraft measurements, a temporary Faraday cage was constructed using aluminium foil.

Scanning electron microscopy (SEM)

Cross-sectional analysis of the coatings was performed using a Thermo Scientific™ Helios™ UXe DualBeam G4 SEM, equipped with an EDX detector and a Plasma Focused Ion Beam (PFIB). The PFIB was used to create precise cross sections of the coatings for detailed analysis. Prior to FIB milling, a platinum layer was sputter-coated onto the surface of the coatings to

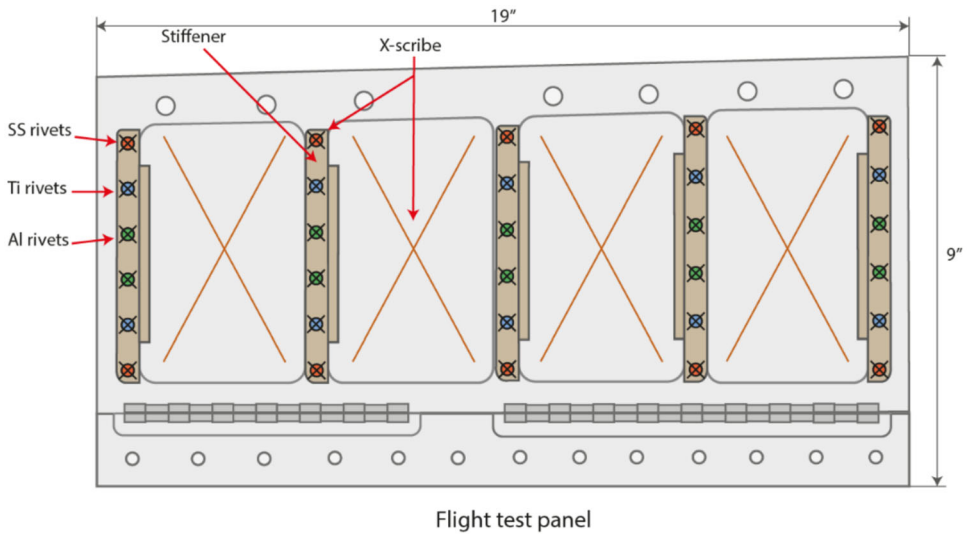

Fig. 2: Schematic example of a flight test panel configuration (dimensions in inches)

protect the top layer from ion beam damage and to facilitate smoother cross-sectional polishing.

To prevent charging effects during SEM imaging, the samples were coated with a carbon layer of approximately 20 nm thick. High-resolution images were acquired at an acceleration voltage of 5 kV with a working distance of 4 mm. For EDX analysis, a higher acceleration voltage of 10–15 kV was used to obtain elemental information.

Attenuated total reflectance Fourier transform infrared spectroscopy (ATR-FTIR)

ATR-FTIR measurements were conducted using a Thermo Nicolet Nexus Fourier Transform Infrared Spectrophotometer, equipped with a mercury-cadmium-telluride (MCT) liquid-nitrogen-cooled detector and a Golden Gate sample holder. Measurements were performed at a spectral resolution of 4 cm^{-1} with 32 co-added scans.

For data analysis, ATR-FTIR spectra were processed using SpectraGryph V1.2 software. The following steps were applied:

I. Advanced baseline correction;
II. Chemometric preprocessing using standard normal variate (SNV) transformation;
III. Spectrum normalization for the chromium- and praseodymium-based epoxy-polyamide coatings relative to the stable aromatic peak at 1606 cm^{-1}.[29, 30] Spectrum normalization for the lithium-based polyurethane coatings relative to the CH_2 bending vibrations at 1445 cm^{-1}, as this band remains relatively stable during weathering.[31]

Results and discussion

This section presents the findings from various tests, including the immersion-, outdoor exposure-, CSST-, and flight test. Additionally, the interrelation between these tests is analysed to provide a comprehensive understanding of the degradation and protection mechanisms of the tested chromate-based coating systems and their proposed alternatives.

Immersion test

The immersion test was conducted using an EIS test setup, serving as a baseline reference for interpreting results from more complex exposure environments. Additionally it enabled direct correlation with findings from previous studies.[26]

EIS measurements

During the immersion test, the electrochemical behavior of the four different coatings was evaluated through EIS measurements at various times of exposure. The impedance modulus |Z| plots for these measurements are shown in Fig. 3.

Figure 3 demonstrates that the impedance modulus Z decreases for all coatings with increasing exposure duration whereby two different degradation trends can be observed.

For the chromate−2 system, the impedance modulus |Z| plot showed a drop in impedance in the mid-frequency range (10^0–10^2 Hz) over immersion time. This decline is likely attributed to changes within the coating, indicating rapid coating degradation, rather than variations in charge transfer resistance at the interface.[32–35] Consistent with an earlier study, the

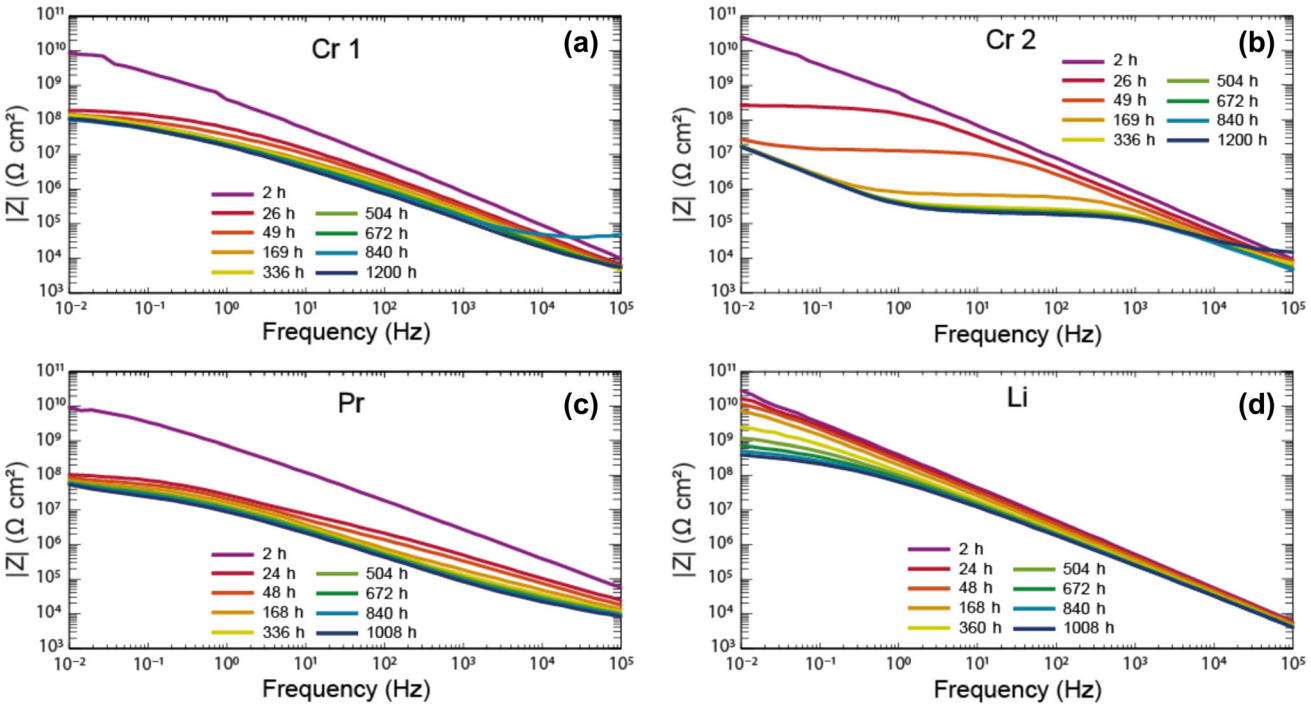

Fig. 3: Impedance modulus |Z| plots for: (a) chromate−1; (b) chromate−2; (c) praseodymium, and (d) lithium coating system during immersion in 0.1 M NaCl aqueous electrolyte

rapid increase in the coating's capacitive behavior is associated with fast electrolyte uptake, which facilitates the dissolution and leaching of embedded corrosion inhibitors.[26] The loss of these inhibitors further increases the coating's capacitance during prolonged immersion, thereby diminishing its barrier properties over time. Interestingly, despite this coating degradation, the impedance modulus |Z| at 0.01 Hz remained relatively high, exceeding 10^7 Ω cm^2. Additionally, after prolonged immersion (> 168 h), the response at $|Z|_{0.01\ Hz}$ indicates capacitive behavior. This suggests that while electrolyte penetration compromised the coating's resistive properties, the underlying charge transfer resistance remained relatively high.[36,37] Since the chromate−2 primer is applied over an anodized oxide layer, it is likely that the electrolyte penetration weakened the coating resistive properties, leading to electrolyte accumulation at the interface of the anodized oxide layer, between the coating and the anodizing oxide layer. The anodized oxide layer still provides high resistance, explaining the capacitive behavior at low frequencies. This indicates that the anodized oxide layer still provides effective corrosion protection. This is further supported by the impedance modulus |Z| value at 0.01 Hz, which remains in the range typically reported at $|Z|_{0.01\ Hz}$ for anodized aluminium substrates (10^6–10^7 Ω cm^2).[38–40]

For the chromate−1, praseodymium and lithium systems, the initial degradation is characterized by a notable decline of the impedance modulus $|Z|_{0.01\ Hz}$ in the low-frequency region. This decrease indicates a gradual reduction in barrier properties. This degradation is likely caused by electrolyte infiltration which fully permeates the coating during immersion testing.[41–43] As the electrolyte penetrates through the pores of the polymer matrix and along the interfaces of the coating pigments, corrosion inhibitors start to dissolve and leach out. This leaching process leads to the formation of voids and interconnected pathways that further compromise the coating's pore resistance over prolonged immersion.[26,44] Despite this degradation, the residual coating resistance, along with the charge transfer resistance at the coating-oxide interface attributed to the protective anodized layer, sustained relatively high impedance values. Even after 1000 h of immersion in 0.1 M NaCl, $|Z|_{0.01\ Hz}$ remained above 5 × 10^7 Ω cm^2.[26,33,45] These results underscore that, despite partial degradation, these systems continue to provide effective corrosion protection over extended exposure periods as seen in the impedance modulus $|Z|_{0.01\ Hz}$ response.[32,33,46]

In addition to the decrease of the modulus |Z| at low frequencies, a decline is also observed in the mid-to-high frequency region (10^3–10^4 Hz) over prolonged immersion time in the chromate−1, praseodymium, and lithium systems. The authors suggest that the observed changes are primarily due to an increase in coating capacitance over extended immersion periods.[26,32,45–47] This effect has already been documented in chromate−1 coating systems, where it is mainly attributed to the leaching of inhibitors, leading to a rise in coating capacitance.[26] A similar mechanism may explain the changes observed in the other coatings. To validate this hypothesis, cross-sectional analyses of the

coatings were conducted using SEM after different immersion times.

SEM-EDX analysis

To investigate pigment dissolution during exposure to the electrolyte, SEM-EDX measurements were conducted on the different coating systems. Figure 4 presents an EDX overlay on the PFIB-milled cross-sectional SEM images, highlighting the elemental composition and spatial distribution of pigments within each coating.

In the chromate−1 system, four distinct elemental combinations were identified, each corresponding to a specific pigment. The presence of Sr, Cr, and O confirms the inclusion of strontium chromate ($SrCrO_4$) as the active corrosion inhibitor. The detection of Si, Al, and O, along with their morphological characteristics, incorporates the use of diatomaceous earth as a filler. Additionally, the combination of Si, Mg, and O indicates the presence of talc ($Mg_3Si_4O_{10}(OH)_2$), whereas Ti and O confirm the incorporation of titanium dioxide (TiO_2).[25, 26]

Similarly, the chromate−2 system also contains talc, strontium chromate, and titanium dioxide. However, unlike the chromate−1 system, diatomaceous earth was not detected. Instead, the presence of Si and O suggests that silicon dioxide (SiO_2) was used as a filler, highlighting a key formulation difference between the two chromate-based coating systems.[48] Additionally, the detection of Mg and O indicates that magnesium oxide was also incorporated into the chromate−2 coating formulation.[49]

In the praseodymium-based coating system, five pigment compositions were identified. The detection of Pr and O suggests the presence of Pr_2O_3 or Pr_6O_{11}, which likely serves as the primary corrosion inhibitor.[50, 51] The presence of Ca and S indicates the inclusion of calcium sulphate (hydrated, $CaSO_4$),[52] while Si and O indicates the presence of silicon dioxide (SiO_2). The detection of Mg and O suggests the use of magnesium oxide (MgO),[49] and Ti and O confirm the inclusion of titanium dioxide (TiO_2).[53]

The lithium coating system exhibited the most diverse pigment composition, with six distinct pigment types identified. The detection of S, Al, Mg, and O suggests the presence of a layered double hydroxide (LDH) pigment based on aluminium and magnesium

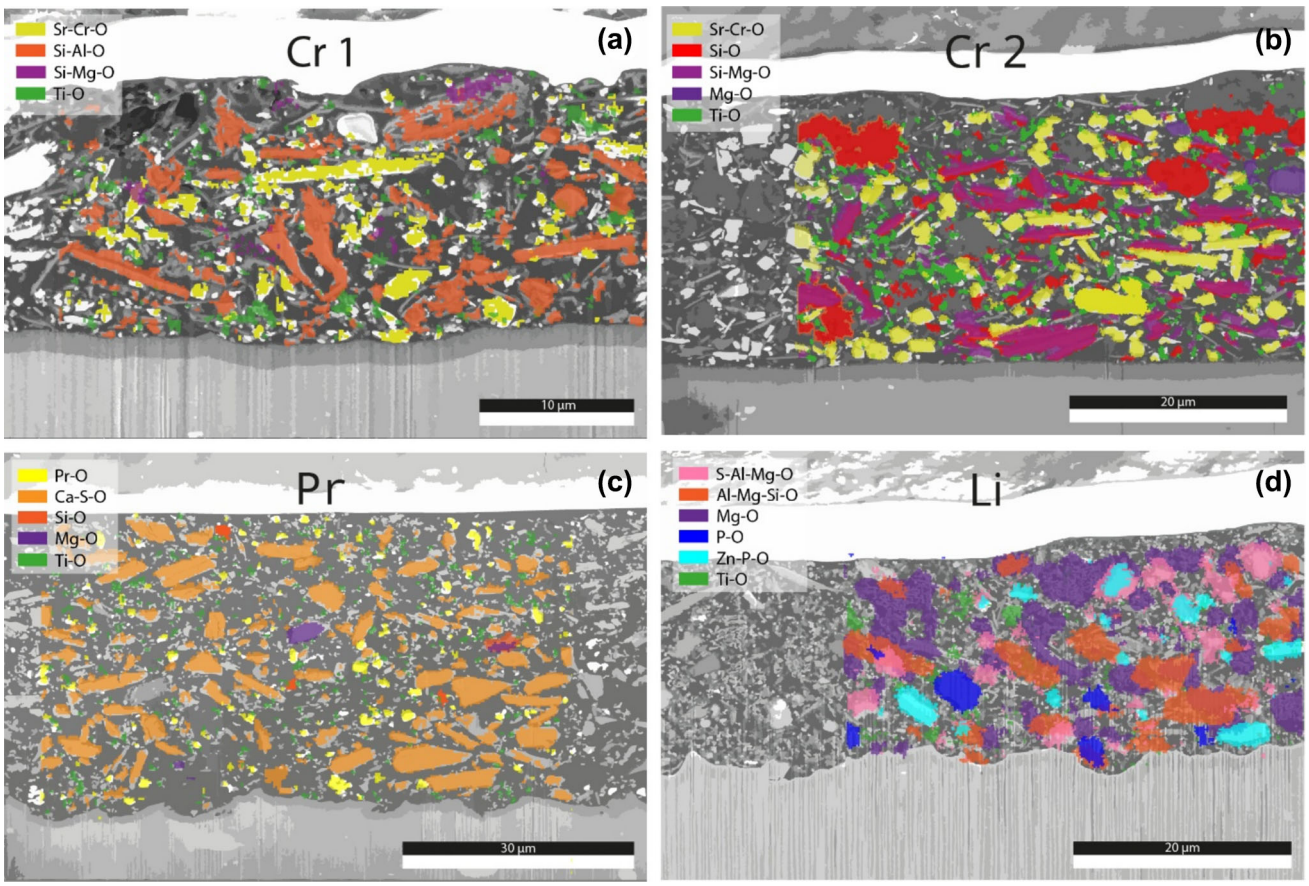

Fig. 4: SEM-EDX analysis of PFIB-milled cross sections of (a) chromate−1, (b) chromate−2, (c) praseodymium, and (d) lithium coating system after 24 h of immersion in 0.1 M NaCl aqueous electrolyte

with sulphate as the intercalating anion ($[Mg_{1-x}Al_{x(OH)2}]_x^+(SO_4)_{x/2}$ mH_2O).[54, 55] Additionally, the presence of Al, Mg, Si, and O suggests the use of ground mica as filler pigments. The detection of Mg and O confirms the presence of magnesium oxide (MgO). Although Li cannot be directly detected using a standard EDX detector, the simultaneous detection of P and O suggests the inclusion of tri-lithium phosphate (Li_3PO_4) as the primary corrosion inhibitor. Similarly, the presence of zinc (Zn), P, and O supports the identification of tri-zinc phosphate ($Zn_3(PO_4)_2$), an additional corrosion inhibitor.[56–58] Lastly, the presence of Ti and O confirms that titanium dioxide (TiO_2) is incorporated as well.

The performance of the different coating systems during immersion in a 0.1 M NaCl aqueous electrolyte reveals distinct pigment dissolution behaviors as shown in Fig. 5.

In the chromate−1 coating, significant pore formation is observed in the upper region of the coating already after only 24 h of immersion. These pores arise from the dissolution of strontium chromate particles, leaving voids within the coating matrix. As immersion time increases, continuous exposure to the electrolyte accelerates the dissolution of strontium chromate. After 1008 h, this depletion process extends throughout the coating, reaching the substrate interface. The extent of pigment depletion is highlighted by a red line, referred to as the depletion front.

A similar phenomenon is observed in the chromate−2 system, where the dissolution of strontium chromate also results in void formation that extends to the substrate after 1008 h. However, unlike the chromate−1 system, certain regions within the chromate−2 coating remain intact, indicating localized areas where strontium chromate has not dissolved. Since both systems share an identical diglycidyl ether of bisphenol A—triethylenetetramine (DGEBA-TETA) epoxy matrix, the difference in depletion behavior is likely due to variations in pigment composition. The chromate−1 coating system contains talc as filler pigments, whereas the chromate−2 coating system incorporates silicon dioxide (SiO_2). This variation may influence water uptake, as water diffusion is likely slower at the polymer-particle interfaces in the chromate−2 system as compared to the chromate−1 system.[59] Consequently, the reduced water ingress in the chromate−2 system delays strontium chromate dissolution, leading to a more gradual depletion process.

In the praseodymium coating system, rapid leaching of inhibitors is observed within the first 24 h of immersion, primarily involving calcium sulphate particles. Due to its high solubility, depletion that extends to the substrate interface becomes apparent within 168-h immersion. By 1008 h, calcium sulphate is completely dissolved throughout the coating, leading to the formation of a porous coating structure. By contrast, praseodymium oxide exhibits lower solubility and undissolved praseodymium-rich particles remain distributed throughout the coating even after prolonged immersion. It appears that calcium sulphate is incorporated primarily to facilitate coating permeability when exposed to moisture, thereby enhancing the release of praseodymium oxide to provide active corrosion protection.[52]

In the lithium-based coating system, only minimal leaching of inhibitors is detected. Even after 1008 h of immersion, depletion is observed only in the uppermost part of the coating. During this process, magnesium oxide particles primarily leach out, while partial dissolution of tri-lithium phosphate and tri-zinc phosphate particles is also observed. The slow dissolution rate of these particles suggests prolonged inhibitor availability under extreme exposure conditions, indicating that this coating could provide sustained active corrosion protection over extended periods.

The SEM analysis confirms that inhibitor leaching during immersion is consistent with the observed decrease in impedance modulus |Z| values in the mid-to-high frequency range (10^3–10^4 Hz).[26] The variations in leaching of inhibitors among the various coating systems correspond with the observed differences in the reduction in impedance modulus |Z| value as shown in Fig. 3.

Outdoor exposure

EIS measurements

During the outdoor exposure tests, quarterly EIS measurements were performed alongside visual inspections. However, many measurements failed due to experimental issues on site, which affected the data usability. The primary challenges encountered during field measurements included: (i) setting up an effective Faraday cage; (ii) selecting suitable electrodes; and (iii) finding a reliable method for pre-wetting the coating prior to the measurements. The successful measurements are presented in Fig. 6.

Despite these challenges, the EIS measurements provide valuable insights. For the chromate coating systems, only a modest decrease of approximately one order of magnitude is observed in the low-frequency range over the 2-year exposure period. Specifically, the impedance modulus $|Z|_{0.01\ Hz}$ decreases from 10^{10} to 10^9 Ω cm^2, which still indicates a well-performing protective coating.[33] Notably, after the coated panels were removed from the exposure rack for the 24-month inspection, the coatings exhibited a full recovery of their barrier properties, with impedance modulus $|Z|_{0.01\ Hz}$ values returning to 10^{10} Ω cm^2. Such a recovery effect has also been observed in previous studies and is likely attributed to the formation of corrosion products, either from the substrate or from the anodization layer, which accumulate within the coating pores, that effectively restores pore resistance.[26, 60, 61] Furthermore, only minimal degradation is detected in the mid-to-high frequency range (10^3–10^4 Hz), suggesting that the capacitance of the chromate coatings

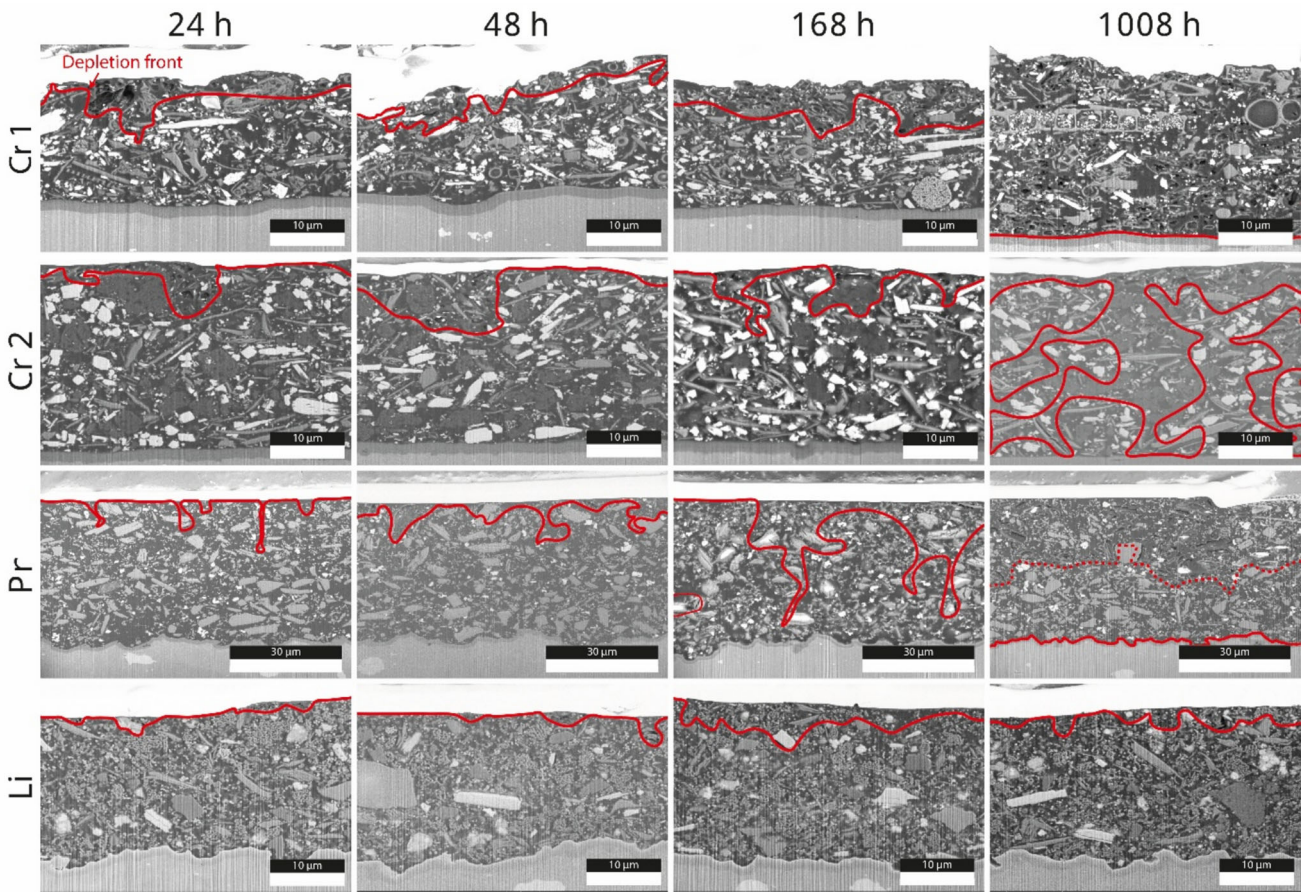

Fig. 5: SEM analysis of PFIB-milled cross sections of organic coatings after various immersion times in 0.1 M NaCl aqueous electrolyte. The red line marks the depletion front within the coating in each image. Magnifications vary slightly to ensure full coating thickness is visible for each coating system

remains largely unaffected by inhibitor leaching. This stability indicates that the inhibitor release mechanism does not significantly compromise the coating's performance, supporting its long-term protective performance.

The praseodymium system exhibits greater degradation during the outdoor exposure test. This is particularly evident when examining the decline in impedance modulus |Z| at low frequencies over time. Specifically, $|Z|_{0.01\ Hz}$ decreases from $10^{10}\ \Omega\ cm^2$ to $5 \times 10^7\ \Omega\ cm^2$, indicating that despite degradation, the coating system still provides effective corrosion protection.[33] Additionally, a significant drop in impedance modulus |Z| is observed in the mid-to-high frequency range (10^3–10^4 Hz), decreasing by approximately one decade. As seen in the immersion test, this reduction suggests inhibitor leaching, which leads to an increase in the coating's capacitance. A slight recovery of the praseodymium coating system is noted in the 24-month measurement, although the extent of recovery was less pronounced as compared to chromate-containing coatings.

During the outdoor exposure test, the lithium coating exhibits a two-order of magnitude decrease in impedance modulus $|Z|_{0.01\ Hz}$, with values dropping to $4 \times 10^8\ \Omega\ cm^2$, which is lower than those observed during the immersion test. A significant reduction in impedance modulus |Z| is also observed in the mid-to-high frequency range (10^3–10^4 Hz), where values declined to approximately $2 \times 10^5\ \Omega\ cm^2$ compared to immersion testing. This suggests that the degradation mechanisms during outdoor exposure are more severe, likely driven by factors beyond electrolyte interaction alone. The increased capacitance, inferred from the decrease in impedance modulus |Z| at mid-to-high frequencies, points to an accelerated leaching of inhibitors. Since outdoor exposure involves less direct electrolyte contact than immersion testing, this accelerated leaching is likely a consequence of polymer degradation, which results in an increased water uptake within the coating.[22] Given that UV radiation is a key environmental factor in outdoor exposure that is absent in immersion testing, it is plausible that UV-induced photo-oxidation leads to polymer scissioning, thereby compromising the coating's integrity. UV-induced degradation has been shown to cause bond scission in polyurethane polymers, particularly at –O–[C=O]–NH– groups, resulting in the formation of –O–

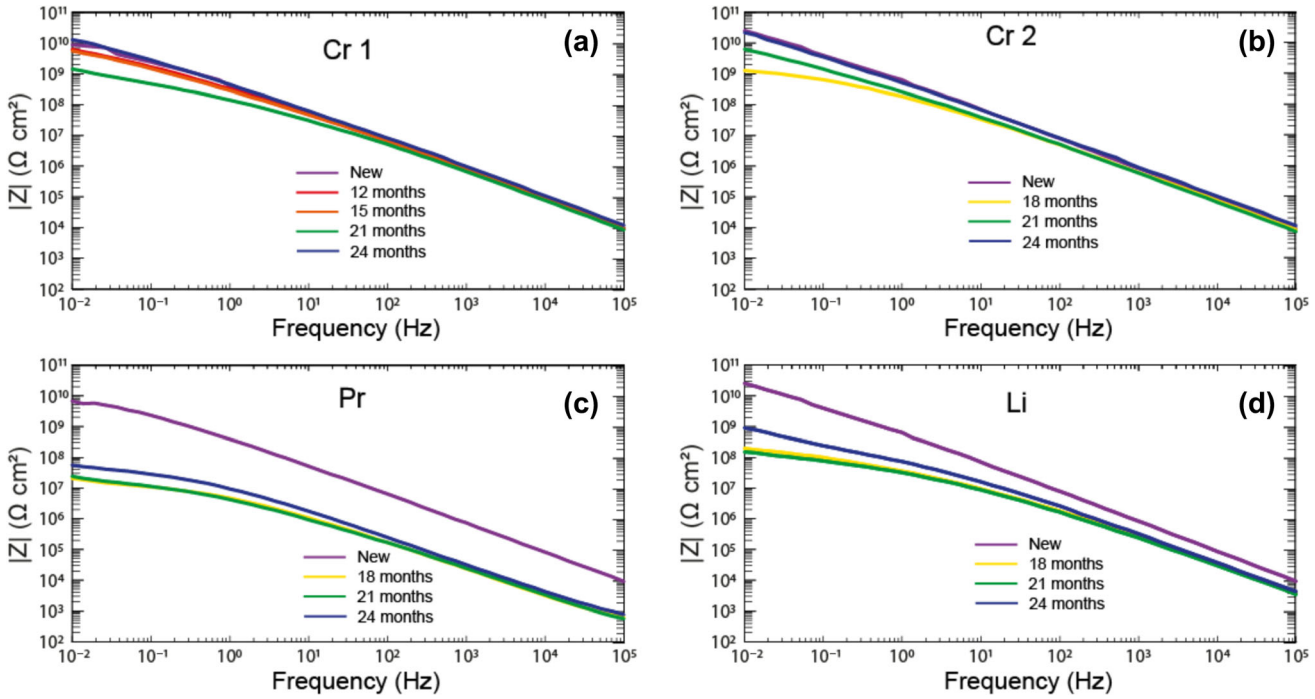

Fig. 6: Impedance modulus |Z| plots for: (a) chromate−1; (b) chromate−2; (c) praseodymium; and (d) lithium coating system during outdoor exposure

[C=O]– and –NH– fragments.[62–64] This scissioning compromises the integrity of the polymer matrix, facilitating moisture ingress and thereby accelerating the depletion of active corrosion inhibitors.

SEM analysis

To understand the electrochemical behavior of the coatings after outdoor exposure, cross sections of the coatings were examined using SEM. The results are shown in Fig. 7.

SEM analysis, as shown in Fig. 7, reveals two distinct degradation mechanisms in the coatings following outdoor exposure: (i) crack formation and (ii) the leaching of corrosion inhibitors, indicated by the depletion front.

Crack formation was particularly destructive in the chromate−1 and praseodymium systems, where cracks extended through the entire coating thickness, reaching the anodized aluminium substrate. The crack formation is likely a result of the combined effects of UV-radiation and moisture exposure.[65–67] UV-radiation induces photo-oxidation within the polymer, leading to polymer chain scissioning. Simultaneously, crosslinking reactions can occur, resulting in a more rigid and densified polymer network with reduced chain mobility.[67] As internal stress within the coating increases due to these UV-induced changes, subsequent moisture exposure exacerbates the problem. Water uptake causes plasticization within the polymer matrix, leading to slight swelling of the coating. However, the limited permeability of water within the polymer network restricts this expansion. In coatings that have undergone extensive UV-induced degradation, the polymer structure loses both its flexibility and its ability to retain the stresses caused by moisture ingress. As a result, the coating can no longer accommodate swelling, which ultimately leads to crack formation.[67, 68]

In addition to crack formation, leaching of corrosion inhibitors was also observed. The leaching process during outdoor exposure is likely influenced by moisture exposure from rainfall and fluctuations in humidity, which affect the time of wetness throughout the testing period.

In the chromate coating system, strontium chromate leaching was clearly visible. However, the extent of leaching was significantly lower than that observed after 1008 h of immersion in electrolyte, leaving a substantial amount of strontium chromate still present within the coating. This indicates that coatings subjected to outdoor exposure experience less continuous electrolyte contact as compared to immersion testing, resulting in a slower inhibitor depletion rate.

Similarly, in the praseodymium system, calcium sulphate leaching was less pronounced after outdoor exposure than after 1008 h of immersion. The leaching front had not yet reached the substrate across the entire coating thickness, suggesting that inhibitor

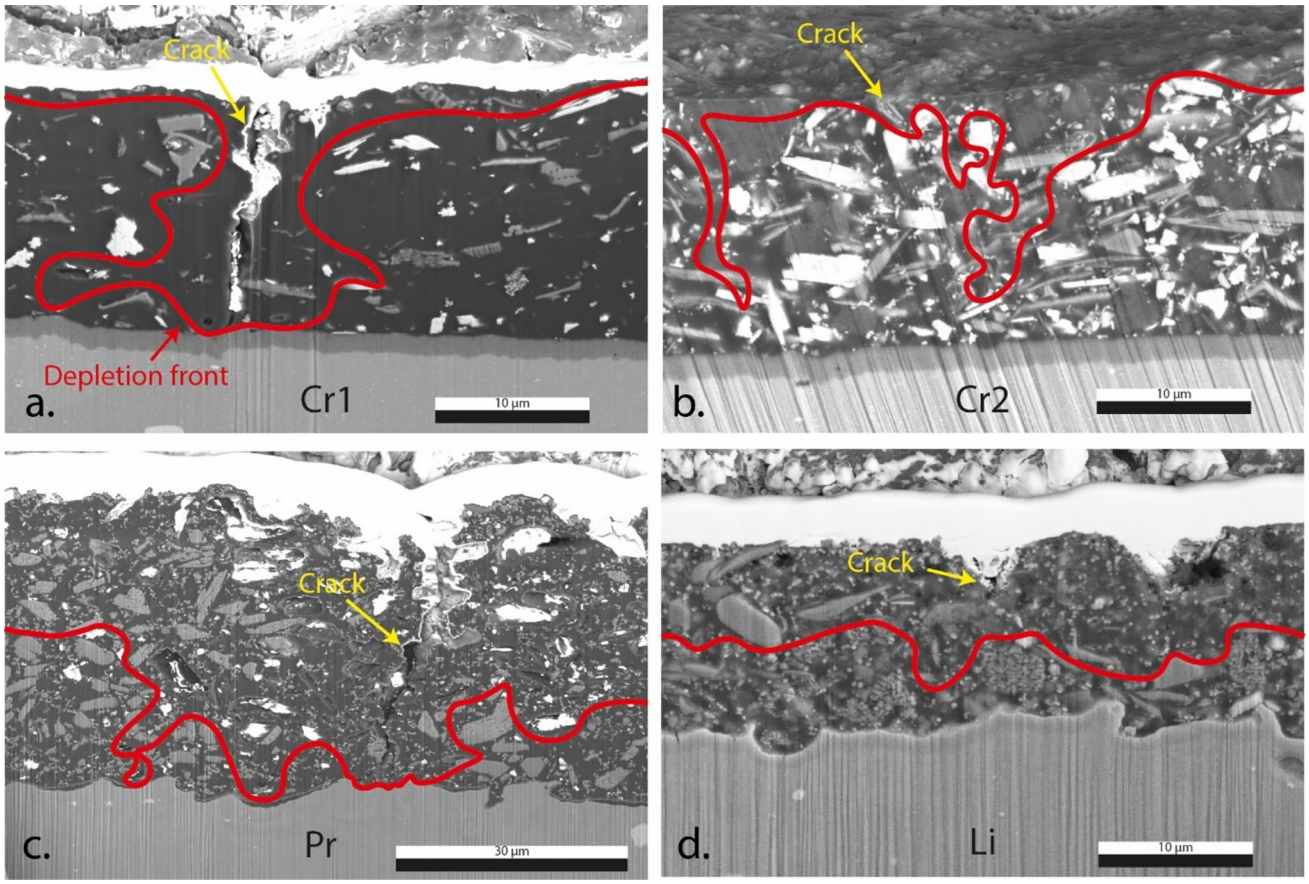

Fig. 7: SEM images of PFIB-milled cross sections of (a) chromate−1, (b) chromate−2, (c) praseodymium, and (d) lithium coating system after unsheltered outdoor exposure, the red lines indicate the depletion front of the leached inhibitors within each coating. Magnifications vary slightly to ensure full coating thickness is visible for each coating system

depletion occurred more gradually. However, among all tested coating systems, the praseodymium coating exhibited the most extensive pigment leaching following outdoor exposure.

In contrast, the lithium system displayed more pronounced leaching after outdoor exposure than after immersion testing. The depletion front extended halfway through the coating thickness, with cracks reaching a similar depth. This correlation suggests that UV-induced cracking facilitated the increased leaching in the lithium system.

Finally, an unexpected observation was made in the chromate−1 coating system, where fewer pigments appeared to be incorporated into the coating after outdoor exposure as compared to the chromate−1 coating system tested during immersion. This variation in pigment concentration could be a result of insufficient stirring of the base component before mixing with the curing agent during paint preparation, potentially leading to inconsistencies in pigment distribution. Uneven pigment dispersion may reduce the local availability of corrosion inhibitors and could also influence the coating's moisture absorption properties, thereby affecting its overall protective performance.[43]

ATR-FTIR analysis

To assess polymer matrix degradation following outdoor exposure, ATR-FTIR analysis was conducted on both the front and back sides of each panel. This approach was chosen to differentiate between UV-induced degradation on the exposed front surface and the comparatively lower UV impact on the back side, which more closely simulates in-service conditions for structural applications. The results were compared with a pristine coating, as shown in Fig. 8. It is important to note that ATR-FTIR analysis-depth is approximately 3 µm, meaning that it focuses only on the degradation at the coating surface.[69]

CHROMATE–1 COATING SYSTEM: In the chromate−1 system, distinct changes in the ATR-FTIR spectra after outdoor exposure are observed at peak positions 3500 cm^{-1}, 1738 cm^{-1}, 1645 cm^{-1} and 1233 cm^{-1}, as well as in the ranges of 3000–2800 cm^{-1}, 1100–1000 cm^{-1}, and 960–860 cm^{-1}, as shown in Fig. 8a.

The increase at the peak at bandwidth 3500 cm^{-1} is attributed to the formation of metal hydroxides, while variations in water adsorption or thermo-oxidation can

be ruled out. Water uptake is unlikely, as all coatings were stored in a dry laboratory environment for several months before IR spectroscopy measurements, ensuring consistent moisture conditions within the coatings.[26] Additionally, thermo-oxidation effects are typically detected within a different ranges (3300–3200 cm^{-1}).[70] The hydroxides are most likely chromium and/or aluminium hydroxides, which may have formed due to moisture ingress and subsequent reactions involving the metallic substrate, its anodized oxide layer or the strontium chromate particles embedded within the coating matrix. This interpretation aligns with previous studies that identified similar metal hydroxides at the coating surface.[26, 71]

The decrease in absorption within the 3000–2800 cm^{-1} and 1100–1000 cm^{-1} ranges can be attributed to a reduction in C–H and Si-O-Si functional groups at the coating surface.[72, 73] This may result from changes in the coating composition due to the formation of metal hydroxides which alter the surface chemistry.[26] The reduction in C–H groups suggests a decrease in polymer bonds, while the lower intensity of Si–O–Si groups indicates a decline in the surface concentration of diatomaceous earth. Another possible contributing factor is chalking due to weathering, where UV-radiation degrades the polymer matrix, thereby reducing the number of detectable C–H groups.[74] This phenomenon is corroborated by the chromate−1 exposure panel as shown in Fig. 9, which reveal significant discoloration and the presence of easily removable, chalk-like coating particles on the surface after outdoor exposure.

The increase in the peaks at 1738 cm^{-1}, 1645 cm^{-1}, and the decrease at 1233 cm^{-1} signifies chemical changes within the polymer matrix. Specifically, the 1738 cm^{-1} peak corresponds to an increase in C=O bonds, the 1645 cm^{-1} peak reflects the formation of amide groups and the 1233 cm^{-1} peak suggests a reduction in C–O–C–C bonds.[70, 75–79] These changes are likely caused by UV-induced degradation,[62–64] where prolonged UV exposure promotes oxidation of polymer chains resulting in scissioning of C–O–C–C bonds and in the formation of carbonyl and amide compounds.[26, 76] This also explains the differences in peak intensities observed between the front and back sides of the exposed panels. The front side, which was directly exposed to sunlight, underwent greater degradation, whereas the back side which was in shadow, received only indirect UV exposure resulting in less severe polymer damage.

Finally, the spectral range 960–860 cm^{-1} can be associated to strontium chromate particles in the coating.[71, 80–83] The decrease in intensity in this region suggests that strontium chromate leaches out of the

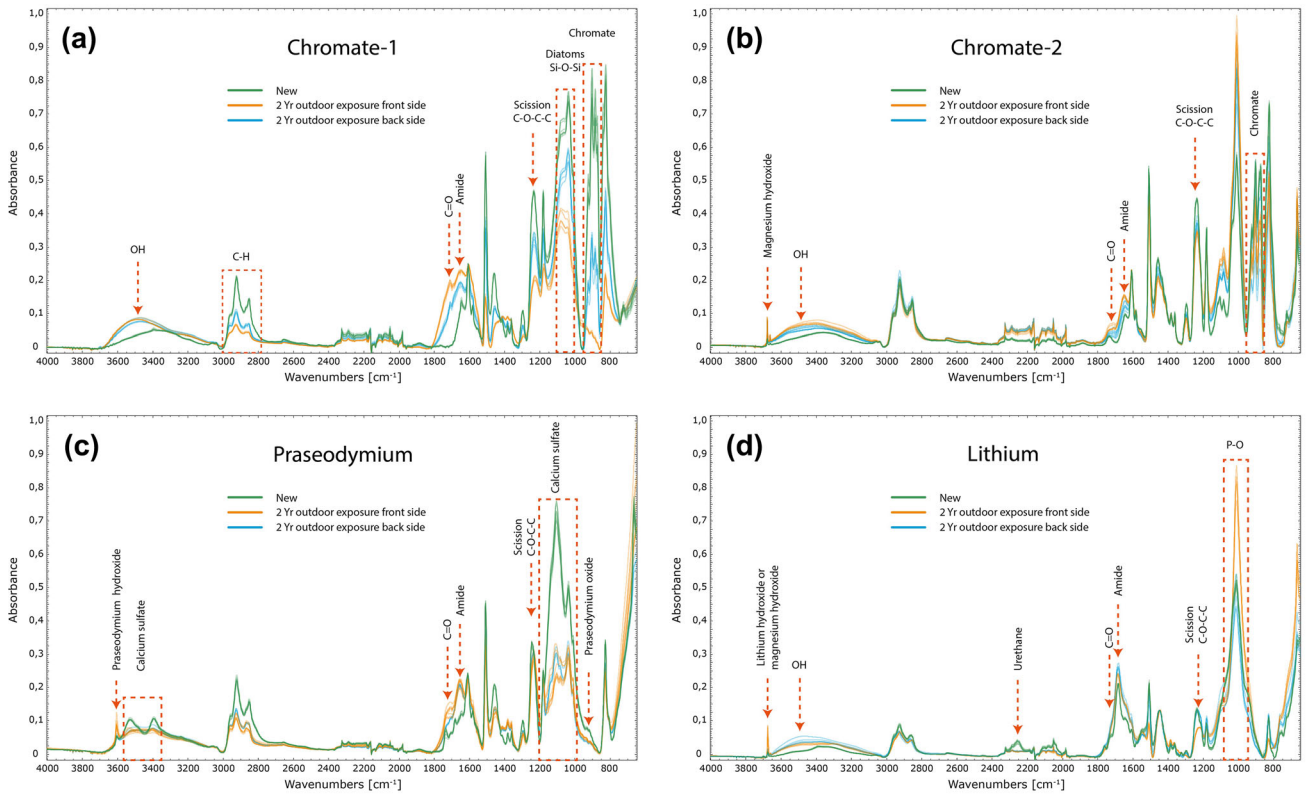

Fig. 8: ATR-FTIR spectra of (a) chromate−1, (b) chromate−2, (c) praseodymium, and (d) lithium coating systems, illustrating the chemical composition changes by comparing newly applied coatings with those exposed to outdoor conditions

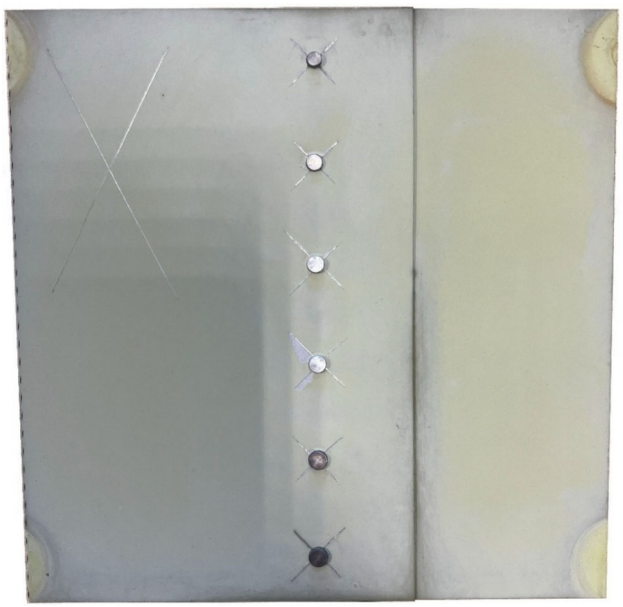

Fig. 9: Chromate−1 panel after two years of outdoor exposure at Naval Air Station De Kooy, showing the chalking effect after environmental weathering

coating during weathering. Since strontium chromate is soluble in moisture, its depletion can be attributed to polymer degradation due to weathering and chalking, as well as moisture ingress caused by rainfall and condensation from day-night cycles. The differences between the front and back sides of the exposed panels further support this hypothesis. The front side, which was directly exposed to rain and UV-radiation, shows near-complete depletion of strontium chromate, whereas the back side, which was not directly exposed to rainfall and UV-radiation, still retains some strontium chromate at the coating surface.

CHROMATE–2 COATING SYSTEM: As shown in Fig. 8b, the chromate−2 system also exhibits an increase in intensity at 3500 cm^{-1}, although to a lesser extent than in the chromate−1 system. This intensity increase suggests the formation of metal hydroxides, most likely aluminium and chromium hydroxides, at the coating surface following outdoor exposure, similar to the chromate−1 coating system.[26]

Furthermore, a reduction in intensity is observed at 1233 cm^{-1}, while increases occur at 1645 cm^{-1} and 1738 cm^{-1}. Similar to the chromate−1 system, these changes indicate that polymer matrix oxidation and chain scission occur in the chromate−2 coating system during outdoor exposure. The intensity variations of these peaks confirm that, as with the chromate−1 system, the front side of the chromate−2 panels has undergone more degradation than the back side.

Additionally, a decrease in intensity is observed in the 960–860 cm^{-1} spectral range, indicating a reduction in strontium chromate due to leaching caused by moisture exposure. However, this reduction is less pronounced than in the chromate−1 system, which is consistent with SEM analysis results after immersion testing. These results demonstrate that the chromate−1 system is more susceptible to complete strontium chromate depletion, as nearly no strontium chromate remained in chromate−1 coating after 1008 h of immersion, whereas the chromate−2 coating retained undepleted areas. The chromate−2 system exhibits less polymer degradation, as indicated by less formation of amide and carbonyl compounds. This suggests that a more intact polymer matrix helps mitigate the complete depletion of inhibitors. As a result, more chromate remains within the chromate−2 system after outdoor exposure.[26]

Finally, after outdoor exposure, the chromate−2 system exhibits an additional peak increase at 3676 cm^{-1}. This peak is likely associated with magnesium hydroxide, suggesting its formation at the coating surface.[84, 85] The increase in magnesium hydroxide can potentially be explained by the presence of magnesium oxide particles in the chromate−2 coating. As magnesium-oxide particles deplete, these may react with moisture, forming magnesium hydroxide, which plays a role in corrosion inhibition by limiting further degradation of the underlying substrate.[49, 86]

PRASEODYMIUM COATING SYSTEM: As illustrated in Fig. 8c, the praseodymium coating system exhibits a decrease in intensity at 3394 cm^{-1} and 3528 cm^{-1} after outdoor exposure. These peaks are associated with calcium sulphate.[87–89] Additionally, the peak at 1105 cm^{-1} is also linked to calcium sulphate[90, 91] The observed intensity reduction indicates that calcium sulphate leaches out of the coating when exposed to moisture, a finding further supported by SEM and EDX results obtained during immersion testing.

A decrease in intensity is also observed at 1233 cm^{-1}, while increases occur at 1645 cm^{-1} and 1738 cm^{-1}.[70, 75–79] Similar to the chromate systems, these spectral changes confirm the occurrence of oxidation and polymer chain scissioning within the matrix. The increased intensity of carbonyl compounds at 1738 cm^{-1} on the front side of the panels indicates a higher degree of polymer matrix oxidation as compared to the back side. This difference is likely attributed to greater exposure to moisture and UV radiation on the front side.

Furthermore, after outdoor exposure, a decrease in intensity is observed at 933 cm^{-1}, a spectral region associated with praseodymium oxide compounds, which may be present as Pr_2O_3 or Pr_6O_{11} within the primer.[92, 93] Simultaneously, an increase in intensity is noted at 3604 cm^{-1}, a peak corresponding to praseodymium hydroxide.[94] These findings suggest that moisture penetration into the praseodymium coating facilitates the leaching of praseodymium oxide, which then transforms into praseodymium hydroxide, praseodymium carbonate, or praseodymium (hydroxyl) carbonate at the coating surface.[51, 52, 95–97] The

deposition of praseodymium hydroxide at 3604 cm^{-1} was more pronounced at the front side of the panels, likely due to longer wetted periods, which enhanced the leaching of praseodymium oxide pigments.

In addition to praseodymium oxide leaching, calcium sulphate also dissolves from the coating. Literature indicates that dissolved calcium sulphate can react with an aluminium substrate, forming aluminium sulphate.[52] Furthermore, calcium sulphate is known to have a synergistic effect on praseodymium gelation, enhancing corrosion inhibition.[52] This suggests that in a damaged praseodymium coating system exposed to moisture, both praseodymium oxide and calcium sulphate dissolve and leach from the coating. At the cathodic areas of the damaged site, the oxygen reduction reaction (ORR) is suppressed by the formation of praseodymium hydroxide, praseodymium carbonate, or praseodymium (hydroxyl) carbonate, with calcium sulphate promoting this protective gelation process.[51, 52, 95–97] Meanwhile, at the anodic sites, aluminium sulphate hydroxide contributes to the formation of a protective oxide layer, resulting from the reaction between calcium sulphate and the aluminium substrate.[52] This mechanism suggests that active corrosion inhibition in the praseodymium system is driven by the combined action of praseodymium species and calcium sulphate, which together protect the substrate.

LITHIUM COATING SYSTEM: In the lithium coating system, as shown in Fig. 8d, an increase in intensity is observed at 3500 cm^{-1}. Similar to the chromium-containing coatings, this peak is attributed to the formation of metal hydroxides. Additionally, a sharp peak at 3676 cm^{-1} is present, which may be associated with the formation of lithium-aluminium LDH[11,98] or magnesium hydroxides, potentially formed from leached magnesium oxide or tri-lithium phosphate particles.[10, 57, 84, 85] These possibilities make it challenging to distinguish the specific protective contributions of lithium-aluminium LDH and magnesium hydroxide at the coating surface. Further research is required to confirm the origin of this peak and to elucidate the role of lithium and/or magnesium in the coating's protective properties.

Additionally, an increase in intensity is observed at 1645 cm^{-1} and 1738 cm^{-1}, along with a decrease at 1233 cm^{-1}. As seen in other coatings, this behavior is attributed to polymer oxidation and scissioning.[70, 75–79] However, in the lithium coating, these intensity changes are less pronounced, indicating that the coating has undergone less degradation. This may be due to the polyurethane-based polymer matrix of the lithium coating, rather than to the epoxy-polyamide-based matrix used in the other coatings tested.

In epoxy-polyamide coatings, hardeners rich in –CN– bonds are commonly used, as seen in the chromate-based coating systems, where triethylenetetramine containing six –CN– groups is used as a hardener. These –CN– bonds have lower bond strength energy, making epoxy-polyamide coatings cured with such hardeners susceptible to UV-induced oxidation and scissioning.[66] Additionally, in polyurethane systems, aliphatic compounds are incorporated to reduce polarity, thereby increasing hydrophobicity within the coating. As a result, polyurethane coatings absorb less moisture than epoxy-polyamide coatings.[99–101] Furthermore, –CN– oxidation under UV radiation is drastically accelerated by moisture.[66] Consequently, epoxy-polyamide coatings exhibit greater oxidation and degradation after outdoor exposure than polyurethane coatings.

Although it was initially assumed that the polyurethane binder might limit the timely release of tri-lithium and tri-zinc phosphate due to its low moisture permeability, ATR-FTIR and SEM analyses revealed that inhibitor leaching was not significantly restricted during outdoor exposure. Sufficient release occurred to provide effective corrosion protection. This observation, supported by previous findings,[22] confirms that polyurethane-based coatings can offer both strong UV-resistance and effective active corrosion inhibition.

Additionally, degradation at 2250 cm^{-1} is associated with the breakdown of polyurethane (–NH–[O=C]–O–).[102] This degradation was observed at both the front and back sides of the panels and was likely caused by moisture ingress.[102] The degradation process initiated the formation of amides (1645 cm^{-1}) and a reduction in carbonyl (C=O) bonds (1738 cm^{-1}), consistent with the degradation mechanism proposed by Liu et al.[102, 103]. Interestingly, the back side exhibited slightly more amide formation than the front, possibly due to pigment leaching, which reduced the pigment-to-polymer ratio more significantly at the front side.

Finally, an increase in intensity is observed at 1015 cm^{-1}, which can be attributed to the presence of phosphate.[57, 104] This phosphate accumulation likely resulted from the leaching of tri-lithium and tri-zinc phosphate pigments from the coating. Additionally, it is possible that the leached phosphate reacted with leached magnesium oxide pigments, forming a magnesium phosphate passivation layer at the coating surface. However, further research is required to confirm this phenomenon.[49, 105, 106]

Cyclic salt spray test (CSST)

EIS measurement

EIS measurements were conducted at various intervals during the CSST, with the results shown in Fig. 10.

For the chromate−1 system, a minimal decrease in Impedance modulus |Z| is observed in the mid-to-high-frequency range (10^3–10^4 Hz) during the CSST, as shown in Fig. 10a. Similar to the behavior observed during immersion testing and outdoor exposure, this decrease is likely due to leaching of strontium chromate which increases the coating's capacitance, thereby affecting the impedance modulus |Z|. The minimal

impedance modulus |Z| drop in this frequency range suggests that strontium chromate leaching was limited during CSST exposure.

By contrast, a significant reduction from 10^{10} to 2×10^{8} Ω cm^2 in the impedance modulus value $|Z|_{0.01\ Hz}$ indicates a notable decline in the coating barrier properties due to CSST exposure. This decrease in impedance is comparable in magnitude to the reduction observed after 1008 hours of immersion in the electrolyte. However, unlike the immersion test, this decline cannot be attributed to inhibitor leaching, as indicated by the distinct behavior of impedance modulus |Z| in the mid-to-high frequency range (10^3–10^4 Hz). These findings suggest that the failure mechanism during CSST is fundamentally different from the degradation processes occurring during immersion testing.

The chromate−2 system exhibited a similar trend as observed in the chromate−1 system, as illustrated in Fig. 10b. A minimal decrease in impedance modulus |Z| in the mid-to-high frequency range (10^3–10^4 Hz) indicates only minor changes in coating capacitance, suggesting minimal leaching of strontium chromate. However, the decrease in impedance modulus $|Z|_{0.01\ Hz}$ follows a different pattern as compared to the chromate−1 system. This pattern resembles the mid-frequency behavior observed during immersion testing, which may indicate that while the coating begins to degrade, the anodized oxide layer still provides effective protection.

The praseodymium system exhibits a small decline of approximately 10^5 Ω cm^2 in impedance modulus |Z| in the mid-to-high frequency range (10^3–10^4 Hz) during CSST exposure. This suggests that fewer inhibitors leached out, leading to a smaller capacitance increase. The limited leaching likely contributed to the coating's improved performance during the CSST as compared to the immersion and outdoor exposure tests. A particularly noteworthy observation was made after 504 h of exposure: despite initial degradation and inhibitor leaching, the praseodymium coating exhibited a full recovery of its barrier properties in the low-frequency range (10^{-2} Hz). However, this recovery effect was no longer observed after 1008 h of exposure, indicating that the recovery mechanism is a transient phenomenon and insufficient to provide long-term protection.

For the lithium system, changes in the impedance modulus |Z| in the mid-to-high frequency range (10^3–10^4 Hz) follow a similar degradation pattern to those observed during outdoor exposure and immersion testing. However, degradation in the low-frequency range (10^{-2} Hz) is less pronounced, with impedance modulus $|Z|_{0.01\ Hz}$ remaining above 10^9 Ω cm^2 after 1008 h of CSST. This impedance modulus $|Z|_{0.01\ Hz}$ value is higher than that observed after outdoor exposure and immersion testing, suggesting enhanced barrier properties during CSST. Additionally, impedance modulus fluctuations were observed during CSST, possibly due to the formation of precipitation products at the surface and within its pores.

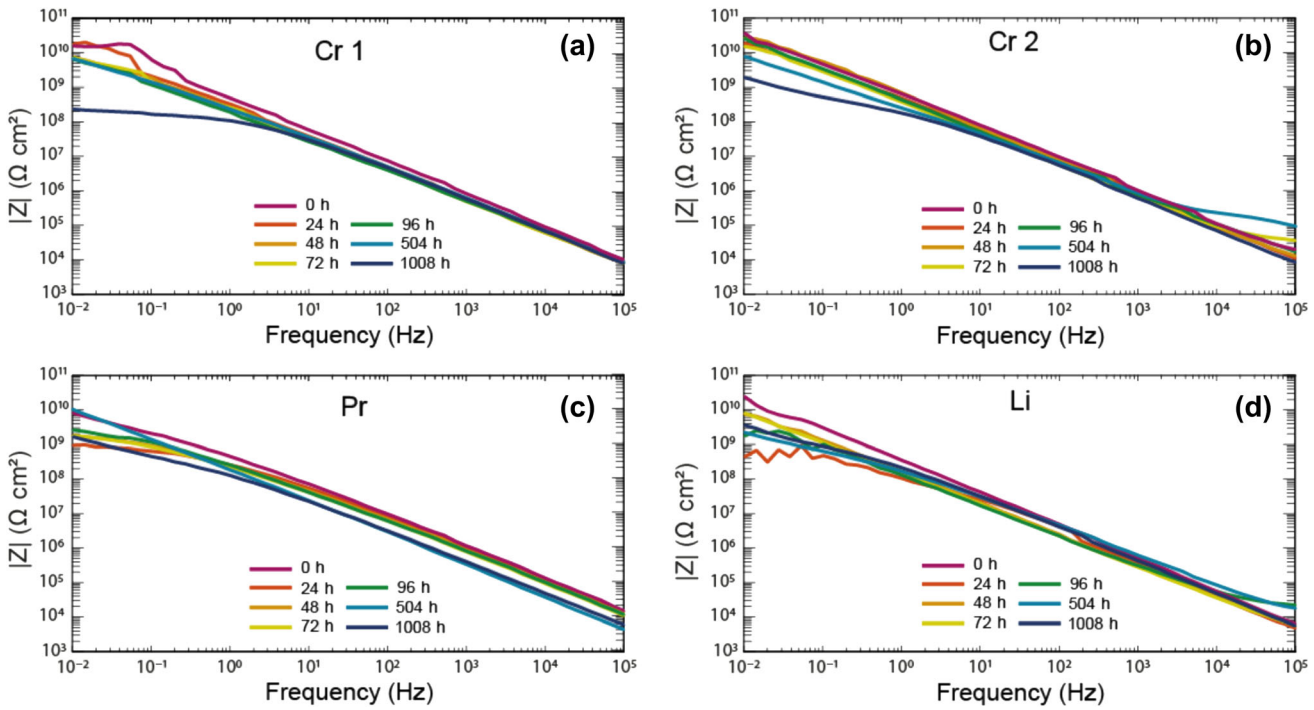

Fig. 10: Impedance modulus |Z| plots for a: (a) chromate−1; (b) chromate−2; (c) praseodymium, and (d) lithium coating system during CSST

Overall, all coatings demonstrated good barrier properties after CSST, as the impedance modulus $|Z|_{0.01\ Hz}$ values in the low-frequency range remained above $10^8\ \Omega\ cm^2$.[32, 46]

SEM-EDX analysis

Figure 11 presents the SEM cross-sectional analysis of the different coating systems after exposure to the CSST.

The primary observation from this analysis is the leaching of corrosion inhibitors from the coatings after CSST, as indicated by the depletion front in Fig. 11. The chromate-based coatings and the lithium coating exhibit similar leaching rates, whereas the praseodymium coating demonstrates a notably faster leaching rate. Importantly, in all coatings, the depletion front has not reached the substrate, indicating that less inhibitors have leached during the CSST as compared to the immersion and outdoor exposure tests.

This difference in leaching behavior can be attributed to the reduced exposure of the coatings to electrolyte during the CSST, which likely slows down the leaching process. Additionally, a more intact polymer matrix may also limit electrolyte penetration, further inhibiting the leaching process. These results explain the superior performance observed in all coating systems during CSST, as evidenced by the EIS measurement, compared to the immersion and outdoor exposure tests.

A particularly noteworthy observation in the lithium system is the formation of a precipitation product on the coating surface after CSST. This finding supports the suggestion that such precipitation product contributes to the fluctuating impedance modulus values observed in Fig. 10d. To better understand the mechanism behind this phenomenon, additional EDX analysis was performed. The EDX analysis, as shown in Fig. 12, overlays the magnesium and oxide mapping results onto the SEM image, revealing that the precipitation product primarily consists of magnesium and oxide compounds. This confirms that the leaching of magnesium oxide particles from the coating leads to the precipitation of magnesium hydroxide, which may

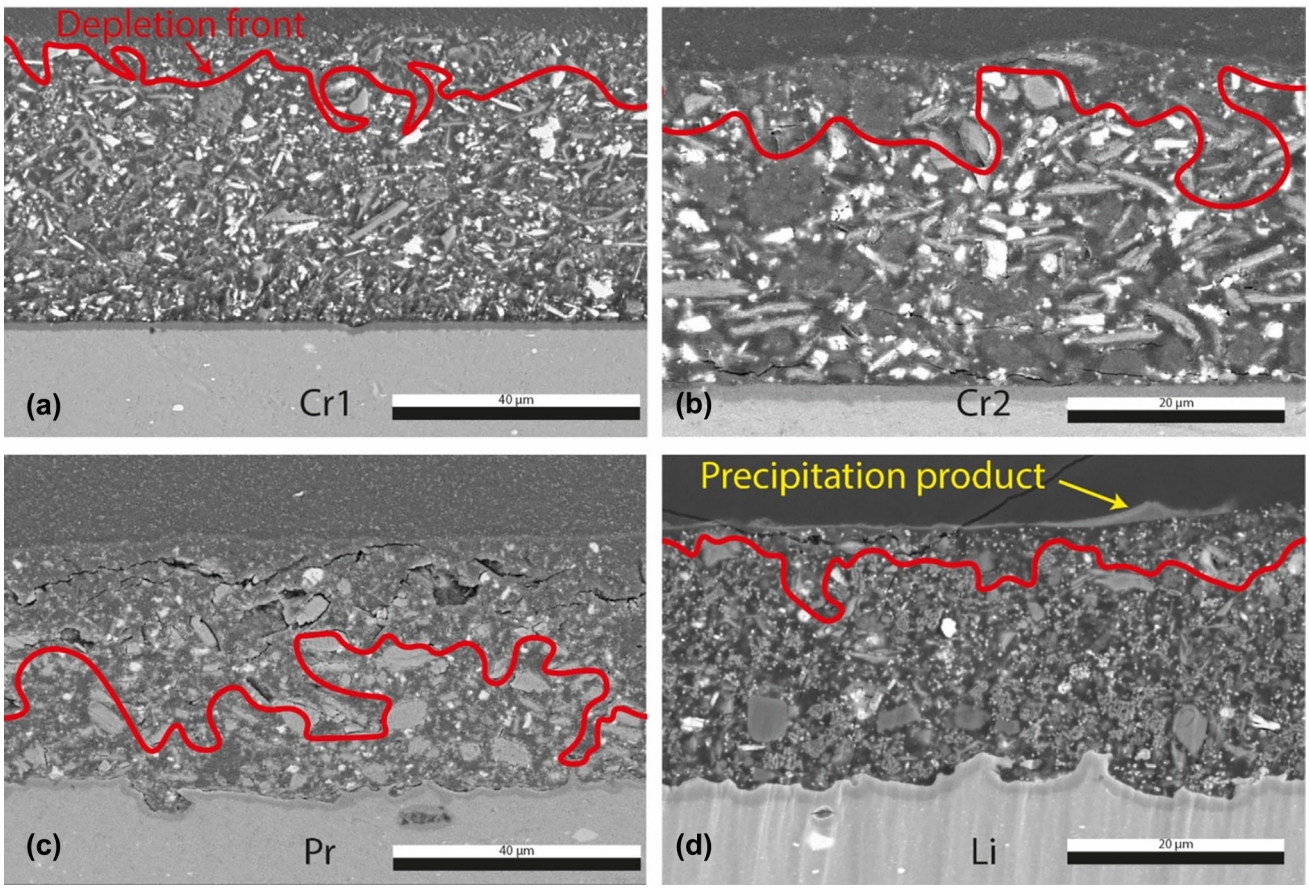

Fig. 11: SEM images of PFIB-milled cross sections of (a) chromate−1, (b) chromate−2, (c) praseodymium, and (d) lithium coating system after CSST, the red lines indicate the depletion front of the leached inhibitors within each coating. Magnifications vary slightly to ensure full coating thickness is visible for each coating system

positively influence the protective performance of the coating during exposure.[49, 86]

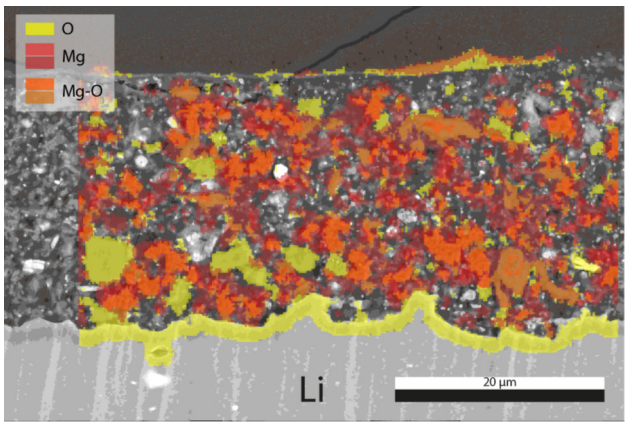

Fig. 12: SEM image of a PFIB-milled cross section of the lithium coating system after CSST, with overlaid EDX maps highlighting the distribution of oxide and magnesium, revealing regions of high and low magnesium intensity

ATR-FTIR analysis

Figure 13 provides the ATR-FTIR analysis results for the coatings after exposure to the CSST.

CHROMATE–1 COATING SYSTEM: After exposure to the CSST, the chromate−1 system exhibits an increase in intensity at 3500 cm^{-1}. As observed in the ATR-FTIR analysis after CSST, as shown in Fig. 13a. This peak is associated with the formation of metal hydroxides, suggesting the precipitation of chromium and aluminium hydroxides on the coating surface after CSST.[26, 71]

The increase in peaks at 1738 cm^{-1} and 1645 cm^{-1}, along with the decrease at 1233 cm^{-1}, indicates that polymer matrix oxidation and scissioning also occur during CSST exposure.[70, 75–79] Unlike outdoor exposure, UV-radiation can be ruled out as a contributing factor to polymer oxidation, as the CSST does not include UV exposure. Additionally, thermo-oxidative degradation is unlikely given that the CSST temperature is maintained at 40° ± 3°C. Instead, it is plausible that the combination of electrolyte exposure, acidity, and the slight temperature increase contributed to polymer scissioning.[107–109] Under these conditions, ether groups in the polymer may undergo hydrolysis in either acidic or alkaline environments, leading to polymer breakdown.[107–110] This confirms that prolonged exposure to moisture alone can induce polymer

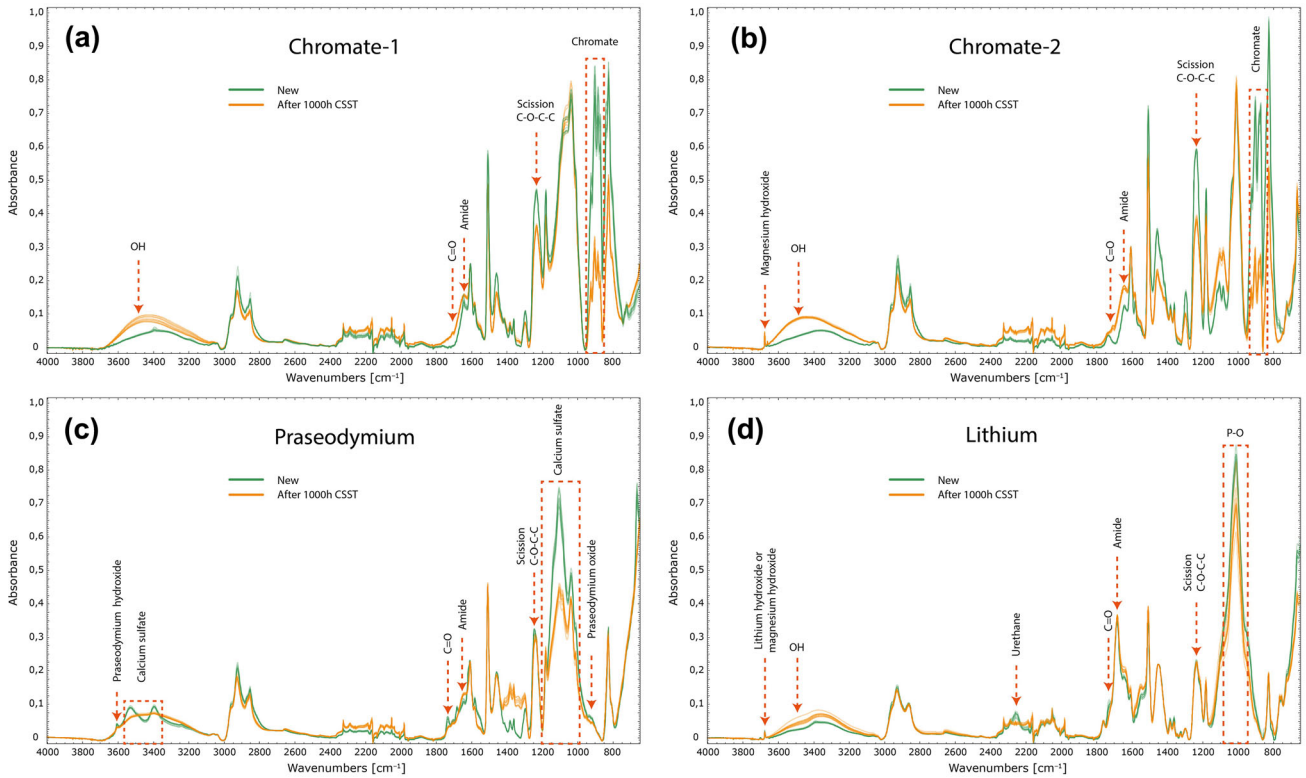

Fig. 13: ATR-FTIR spectra of (a) chromate−1, (b) chromate−2, (c) praseodymium, and (d) lithium coating systems, illustrating the chemical composition changes by comparing newly applied coatings with those exposed to CSST

degradation through oxidation and scissioning in organic coatings.

Finally, the ATR-FTIR analysis of the chromate−1 system reveals a significant decrease in the spectral range between 960 and 860 cm^{-1} after CSST exposure. As seen earlier, this reduction is attributed to the leaching of strontium chromate, a finding further supported by SEM analysis.[71, 80–83]

CHROMATE–2 COATING SYSTEM: The chromate−2 system exhibits degradation behavior similar to that of the chromate−1 system, as shown in Fig. 13b. Polymer scissioning in the epoxy matrix, leaching of strontium chromate and metal hydroxide formation, is all clearly observed. The primary distinction between the chromate−2 and chromate−1 systems is the presence of a peak at 3676 cm^{-1}. This peak is attributed to the formation of magnesium hydroxides, likely resulting from the leaching of magnesium oxide particles embedded in the chromate−2 coating.[49,86]

PRASEODYMIUM COATING SYSTEM: As illustrated in Fig. 13c, the praseodymium coating system exhibits a clear reduction in the peaks at 3394 cm^{-1}, 3528 cm^{-1}, and 1105 cm^{-1}. These peaks are associated with calcium sulphate, indicating its leaching during CSST exposure.[87–91] In contrast, no significant changes are observed for the praseodymium oxide peak (933 cm^{-1}) or the praseodymium hydroxide peak (3604 cm^{-1}).[92–94] This absence suggests that the dissolution of praseodymium oxide (Pr_2O_3 or Pr_6O_{11}) is limited, likely due to its inherently low solubility and the restricted exposure of the coating to electrolytes during CSST.[111] As a result, the leaching of praseodymium-based inhibitors and the associated passivation processes appear to be less pronounced under these conditions.

Furthermore, the praseodymium system shows minimal polymer degradation after CSST exposure. The absence of a significant reduction in the peak at 1233 cm^{-1}, combined with only slight increases at 1645 cm^{-1} and 1738 cm^{-1}, indicates that oxidation and scissioning of the polymer matrix are limited.[70, 75–79] This implies that the epoxy-polyamide matrix in the praseodymium system is more resistant to hydrolytic degradation compared to the epoxy-polyamide polymers used in the chromate-based systems.

LITHIUM COATING SYSTEM: As shown in Fig. 13d, the lithium coating system exhibits negligible changes in the peaks at 1233 cm^{-1}, 1645 cm^{-1}, and 1738 cm^{-1}, indicating that polymer oxidation and scissioning due to hydrolysis are minimal.[70, 75–79] However, degradation of urethane bonds (2250 cm^{-1}) is observed, although this does not result in significant amide formation (1645 cm^{-1}).[70, 75–79, 102]

A particularly notable observation is the change in the peak at 1015 cm^{-1}, which suggests the leaching of tri-lithium or tri-zinc phosphate pigments from the coating.[57, 104] Interestingly, instead of an expected increase, a decrease in this peak is observed. This may be due to the absence of magnesium phosphate

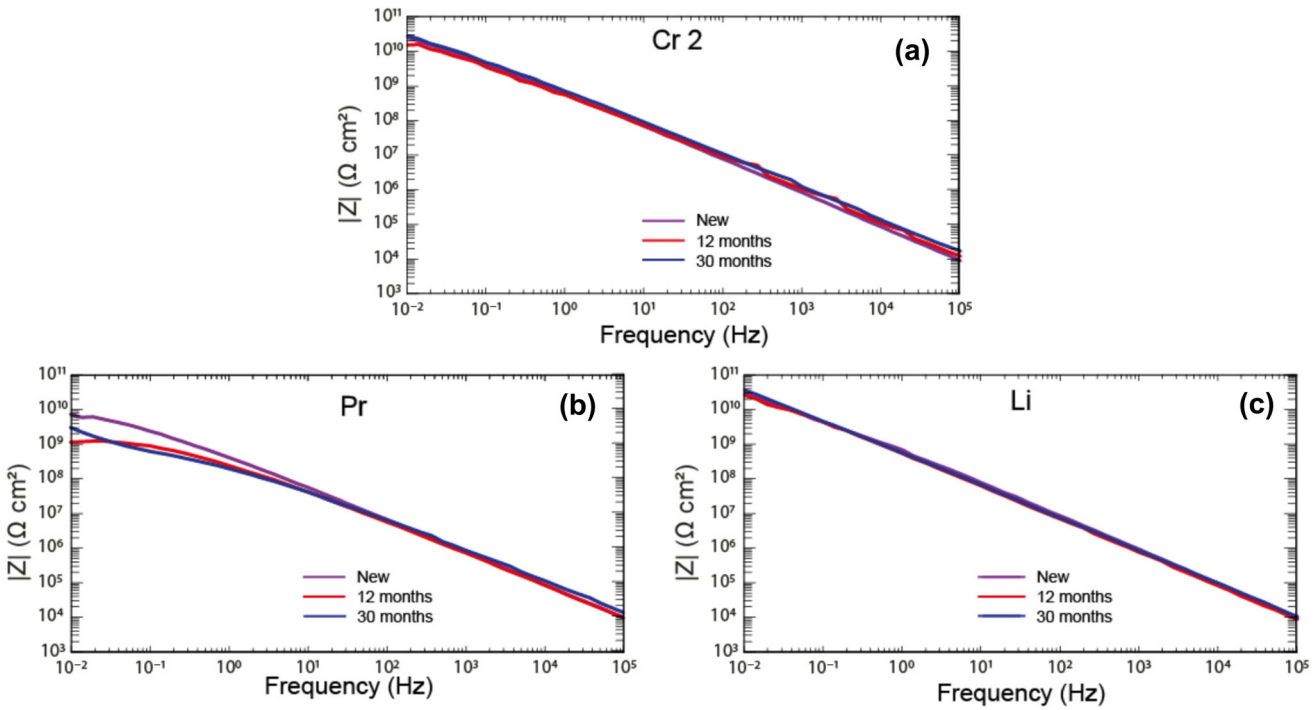

Fig. 14: Impedance modulus |Z| plots for: (a) chromate−2; (b) praseodymium, and (c) lithium coating system during flight testing

formation on the panels after CSST exposure. Additionally, lithium and/or magnesium hydroxides (3676 cm^{-1}) are not detected on the coating surface.[98] One possible explanation is that the formation of a salt crust during CSST may have interfered with these processes, preventing the precipitation of Li-Al LDH, magnesium hydroxide, and magnesium phosphate at the coating surface.

Flight test analysis

EIS measurements

The EIS measurements conducted during and after the flight tests are shown in Fig. 14 as impedance modulus |Z| plots.

The results indicate that the chromate−2 and lithium coating systems exhibited negligible changes in impedance modulus $|Z|_{0.01\ Hz}$ throughout the entire flight test period. This stability suggests that these coatings maintained their protective properties, providing excellent corrosion resistance. In contrast, the praseodymium system displayed a one-order-of-magnitude decline in impedance modulus $|Z|_{0.01\ Hz}$ over time, indicating minor degradation. Nevertheless, the impedance modulus value $|Z|_{0.01\ Hz}$ remained above $10^9\ \Omega\ cm^2$, demonstrating that the praseodymium coating still provided effective protection during the flight test period.[32, 46]

For all coating systems, the impedance modulus |Z| in the mid-to-high frequency range (10^3–10^4 Hz) remained largely unchanged, suggesting that no substantial inhibitor leaching occurred over the 2.5-year test period. The stable values further indicate that inhibitor leaching did not significantly alter the coating's capacitance or influence the impedance modulus |Z| response in this frequency range. These findings suggest that the coatings experienced minimal exposure to electrolytes during flight testing, preserving their active protective performance.

SEM analysis

Cross-sectional images of the coatings, prepared using PFIB milling after 2.5-year of flight testing, are presented in Fig. 15.

The SEM analysis results, as depicted in Fig. 15, reveal that the chromate−2 and lithium coating systems remained nearly intact after flight testing, with only minor depletion of inhibitors. By contrast, the

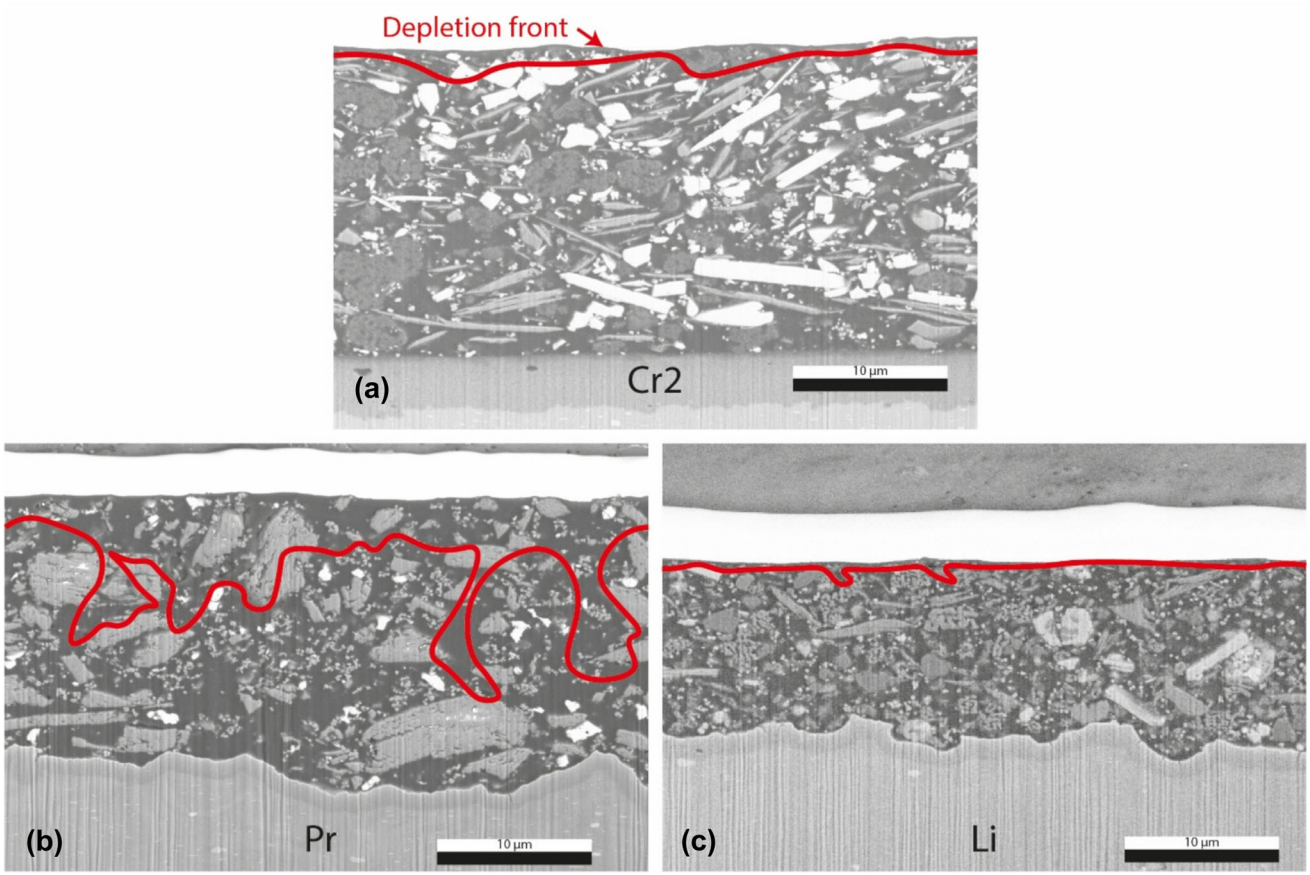

Fig. 15: SEM images of PFIB-milled cross sections of (a) chromate−2, (b) praseodymium, and (c) lithium coating system after flight testing, the red lines indicate the depletion front of the (partially) leached inhibitors within each coating

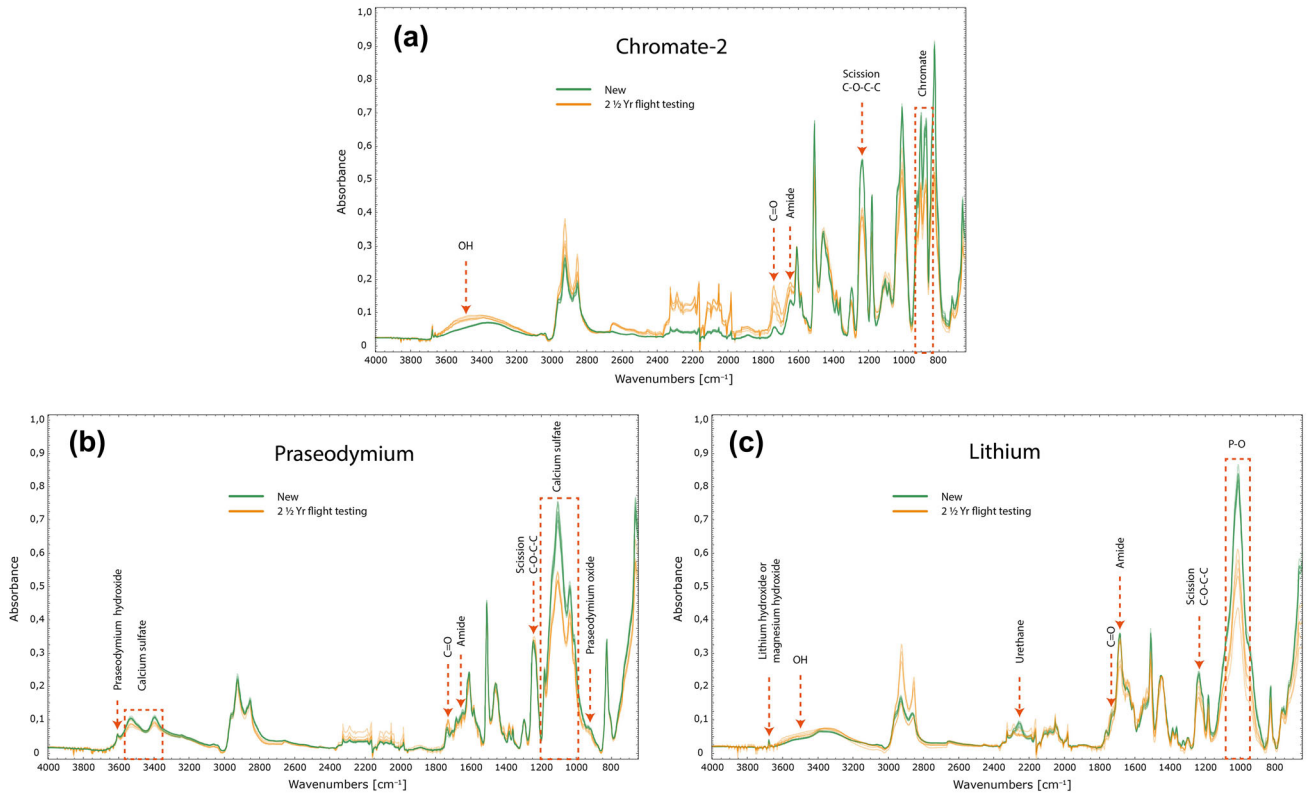

Fig. 16: ATR-FTIR spectra of (a) chromate−2, (b) praseodymium, and (c) lithium coating systems, illustrating the chemical composition changes by comparing newly applied coatings with those exposed to flight testing

praseodymium coating exhibited more pronounced inhibitor depletion, suggesting a higher degree of electrolyte exposure, leading to partial leaching of calcium sulphate particles. However, this leaching did not result in significant changes in the impedance response, as confirmed by the EIS measurements. It is likely that the degradation becomes apparent only as electrolyte pathways penetrate deeper into the coating and reach the metal substrate. Over time, these pathways may expand, potentially accelerating degradation as observed in EIS measurements during outdoor exposure or CSST.

ATR-FTIR analysis

The ATR-FTIR spectra comparing coatings after 2.5-year of flight testing with newly applied coatings are shown in Fig. 16.

After flight testing, the chromate−2 system exhibited a significant decrease at the 1233 cm^{-1} peak, along with increased signals at 1645 cm^{-1} and 1738 cm^{-1}, as shown in the ATR-FTIR measurement in Fig. 16a. These spectral changes indicate oxidation and scissioning of the polymer matrix, consistent with previous findings.[70, 75–79] Additionally, the reduction in 860–960 cm^{-1} region indicates the leaching of strontium chromate, while the increase at 3500 cm^{-1} is linked to the formation of chromium and aluminium hydroxide on the coating surface.[26, 70, 71, 80–83] These observations align with SEM analysis, which confirmed chromate leaching at the coating surface due to electrolyte exposure. The combination of electrolyte exposure and the thermal stress during flight testing likely contributed to the oxidation-induced polymer scissioning.[26]

Conversely, in the praseodymium system, the peaks at 1233 cm^{-1}, 1645 cm^{-1}, and 1738 cm^{-1} remained stable after flight testing, as shown in Fig. 16b. This stability indicates that the praseodymium coating exhibited minimal polymer degradation via scissioning or oxidation.[70, 75–79] However, significant leaching of calcium sulphate is observed at 3528 cm^{-1}, 3394 cm^{-1}, and 1105 cm^{-1}.[90, 91] Notably, this leaching was confined to the upper 3 μm of the coating layer, consistent with the limited penetration depth of ATR-FTIR.[69] By contrast, the leaching of praseodymium oxide (933 cm^{-1}) was negligible, and no formation of praseodymium hydroxide (3604 cm^{-1}) was observed.[92–94] These findings suggest that the coating experienced limited electrolyte exposure during flight testing, restricting the dissolution of praseodymium oxide due to its low solubility. Despite this limited exposure, the rapid leaching of calcium sulphate had a notable impact on electrochemical performance, con-

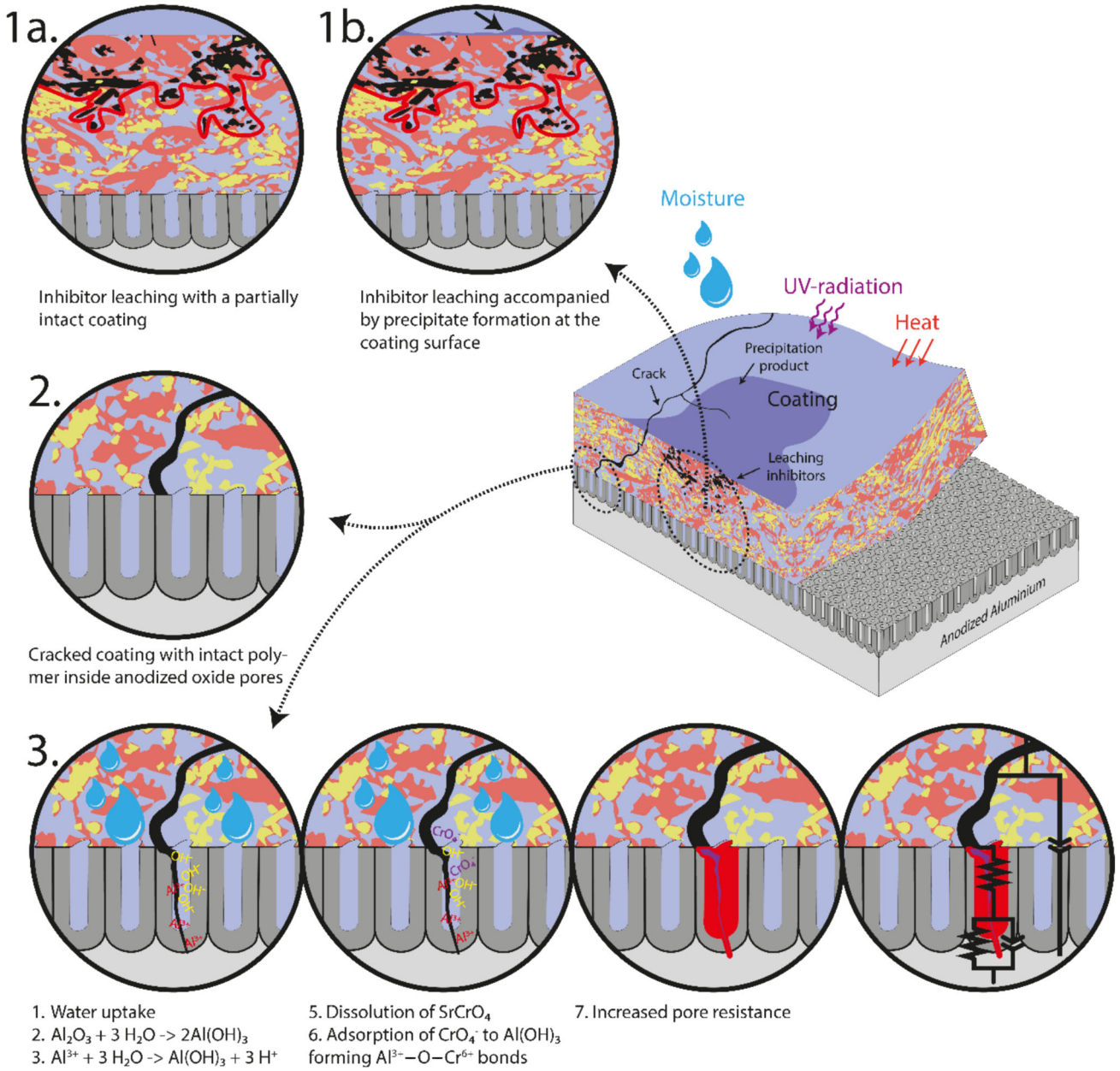

Fig. 17: Proposed degradation and protection mechanisms: (1a) Inhibitor leaching from a partially intact polymer matrix; (1b) Inhibitor leaching accompanied by precipitate formation at the coating surface; (2) Cracked coating with intact polymer embedded in the anodized oxide pores; and (3) Enhanced pore resistance in the anodized oxide layer due to chromate activity

tributing to a reduction in impedance modulus $|Z|_{0.01\ Hz}$ of approximately one decade.

As shown in Fig. 16c, the lithium system exhibited a decrease in the 1233 cm^{-1} peak after flight testing, indicating scission in the polymer matrix.[70, 75–79] A reduction at 2250 cm^{-1} was also observed, suggesting degradation of the polyurethane polymer.[102] Interestingly, the peak at 1645 cm^{-1} remained stable, indicating that polymer degradation did not significantly affect the formation of amide groups in the lithium coating. Additionally, the leaching of tri-lithium and/or tri-zinc phosphate was identified at 1015 cm^{-1}, confirming moisture penetration into the coating during flight testing.[57, 104] This moisture uptake, combined with thermal stress, likely contributed to surface-level degradation of the polyurethane matrix.[26, 62, 112]

Unlike in outdoor exposure tests, the lithium coating system did not exhibit the formation of magnesium phosphate, magnesium hydroxide, or Li-Al LDH protection layers at the coating surface after flight testing. This difference may be attributed to a reduced leaching of inhibitors during flight testing, which could

have limited the availability of reactants necessary for the formation and deposition of these protective layers.

ATR-FTIR analysis after flight testing highlights the role of thermo-oxidation and hydrolysis in polymer degradation. These two processes are critical during flight testing and have a more pronounced impact on the lithium polyurethane-based coating as compared to the praseodymium epoxy-polyamide-based coating evaluated in this study. Further research is recommended to investigate the effects of hydrolysis and thermo-oxidation on polymer scissioning in aerospace coatings. Enhancing the resistance of organic coatings to these degradation mechanisms could improve their long-term barrier performance and durability in flight environments.

Changing testing protocols for reliable performance prediction

The 2.5-year flight test results show that the coatings remain largely intact, with minimal inhibitor leaching and no significant barrier degradation. This aligns with expectations for coatings under typical operational conditions, where exposure to harsh environmental stressors, such as prolonged UV radiation, frequent wetting, and aggressive chemical contact, is relatively limited. These results therefore provide a valuable and realistic baseline for evaluating early-stage coating performance of structural aircraft coatings.

When compared to previously published data on the chromate−1 coating system after more than 35 years of in-service exposure,[25, 26] a notable similarity is observed: both the short- and long-term samples exhibit high impedance values and minimal capacitive degradation. SEM cross-sectional analysis of both sample sets confirms that inhibitor leaching is not the primary degradation mechanism in intact coatings. Instead, ATR-FTIR reveals polymer chain scissioning, driven by thermal oxidation and hydrolysis, as the primary mechanism. Importantly, this process is already detectable after just 2.5 years, underscoring the sensitivity and diagnostic value of ATR-FTIR in detecting early-stage chemical changes in the polymer matrix.

The long-term durability of the chromate−1 coating system appears to be closely linked to its ability to restore pore resistance. Research, including the outdoor exposure results, suggested that the formation of aluminium corrosion products, combined with chromate adsorption, creates a dipolar structure within the coating pores that impedes electron transfer.[25, 71, 113] This barrier restoration mechanism can partially offset the effects of polymer degradation in chromate-containing coating systems. By contrast, chromate-free coating systems may lack such restorative mechanisms, increasing their susceptibility to long-term failure and emphasizing the need for further investigation into their long-term performance.

Furthermore, in-service coating failures are typically driven by localized degradation rather than by uniform deterioration. Studies have shown that moisture accumulation, especially around fasteners and in geometrically complex areas such as lap joints and crevices, can lead to localized inhibitor leaching and corrosion initiation, even in chromate-containing systems.[22, 25]

To improve predictive accuracy, revised testing protocols should incorporate stressors such as thermal oxidation, to replicate polymer degradation mechanisms observed during in-service exposure. Furthermore, these protocols should address localized degradation phenomena by incorporating targeted laboratory experiments. This includes cyclic salt spray testing using purpose-designed samples that mimic real-world structural features, such as fasteners, dissimilar material joints, and crevices, as proposed in a previous study.[22] That study also recommends specific CSST parameters that should be adjusted to better simulate service conditions and enhance the reliability of performance predictions.

However, several key aspects remain insufficiently explored to support the development of a robust testing protocol that reliably predicts long-term service performance. Future research should focus on clarifying the relationship between polymer degradation, particularly chain scissioning, and the long-term protective capabilities of coating systems. In chromate-containing coatings, this form of degradation has not proven critical, largely due to their inherent barrier restoration mechanisms. By contrast, chromate-free systems may lack such barrier restoration properties, making these more susceptible to long-term performance loss. While advanced polymer chemistries offer the potential to mitigate these challenges through enhanced resistance to thermal oxidation and hydrolysis, their long-term effectiveness and contribution to overall coating durability are still not fully understood.

Proposed degradation and protection mechanisms

The results of the EIS, SEM, and ATR-FTIR analyses provide valuable insights into the degradation mechanisms of various coating systems. Observations from the different exposure tests have led to the identification of several mechanisms explaining how these systems degrade over time, the factors influencing this process and how these continue to provide corrosion protection. These mechanisms are summarized in Fig. 17.

Mechanism 1: Inhibitor leaching with a partially intact organic coating

The first mechanism describes the degradation of structural coatings driven by the leaching of corrosion inhibitors when exposed to moisture (Fig. 17, 1a). As these inhibitors dissolve and leach out from the coating

matrix, voids and pores are created, significantly reducing the coating barrier properties by increasing its permeability to water and electrolytes. The rate of inhibitor leaching is primarily determined by the solubility of the inhibitors and the diffusivity of water and electrolytes through the polymer matrix. The diffusion properties of the polymer are closely linked to the integrity of its chemical structure.

UV-radiation plays a major role in degrading these chemical bonds, inducing chain scissioning in the polymer and creating pathways that facilitate water ingress. Furthermore, hydrolysis and thermo-oxidative processes, also able to degrade the chemical bonds by scissioning, enable increased water diffusion and inhibitor leaching. Over time, this cumulative loss of inhibitors and rising porosity compromise the coating's ability to act as a barrier, ultimately reducing its effectiveness in protecting against corrosion.

Despite these degradation processes, certain areas of the organic coating remain intact and continue to deliver corrosion protection. The degradation does not fully penetrate through the organic coating to reach the metal substrate. This observation is supported by the study's findings, which demonstrate that outdoor exposure caused significant damage to the polymer matrix, primarily due to UV-radiation. UV exposure led to extensive degradation of the polymer bonds. However, the lithium and chromate−2 coating systems exhibit strong resistance to UV-induced degradation. SEM analysis revealed that cracks formed in these coatings do not propagate towards the substrate, preserving the integrity of the coating system. This is further supported by EIS measurements, which showed impedance modulus values $|Z|_{0.01\ Hz}$ exceeding $10^8\ \Omega\ cm^2$. These high impedance modulus values confirm that the coatings maintained robust barrier properties and continued to provide excellent corrosion protection, even under harsh conditions.

During the CSST, polymer degradation occurs mainly through hydrolysis, resulting in significantly reduced leaching of inhibitors as compared to outdoor exposed coating systems. No cracks were observed in any of the tested coating systems. Instead, degradation was predominantly attributed to the inhibitor leaching itself, consistent with the proposed mechanism. EIS measurements showed impedance modulus values $|Z|_{0.01\ Hz}$ exceeding $10^9\ \Omega\ cm^2$, indicating that the polymer matrix embedded within the anodized oxide pores remained intact. Furthermore, the sections of the coating unaffected by leaching likely contributed to the strong barrier properties observed.

In the lithium system, SEM analysis following CSST revealed the formation of corrosion product on the coating surface (Fig. 17, 1b). These surface deposits may have further enhanced the impedance modulus values $|Z|_{0.01\ Hz}$ observed during EIS measurements. However, prolonged exposure could compromise the integrity of this corrosion product layer, potentially causing fluctuations in impedance over time.

Flight testing exhibited the lowest levels of inhibitor leaching among all tested conditions. However, ATR-FTIR analysis did indicate more extensive polymer matrix damage as compared to CSST. This discrepancy may result from reduced electrolyte exposure during flight testing, which minimized inhibitor leaching while thermo-oxidation further degraded the polymer structure. The reduced inhibitor leaching during flight testing contributed to the high impedance modulus values $|Z|_{0.01\ Hz}$, which exceeded $10^9\ \Omega\ cm^2$ after the test.

All coatings exposed to CSST and flight testing, as well as the lithium and chromate−2 systems subjected to outdoor environments, align with this first mechanism. In these cases, although the leaching of inhibitors caused some damage to the coatings, it did not compromise their barrier properties. Instead, the intact polymer regions within the organic coating and the anodized oxide layer with polymer embedded inside its pores, effectively prevented corrosion of the aluminium substrate to occur.

Mechanism 2: Cracked coatings with intact polymer in anodized oxide pores

In this second proposed mechanism, the polymer matrix within the organic coating is completely degraded due to UV radiation, hydrolysis, and/or thermo-oxidation processes. Despite this extensive degradation, the anodized oxide layer, with the polymer embedded inside its pores, continues to provide sufficient corrosion protection. Evidence of this is observed during the outdoor exposure tests, particularly for the praseodymium and chromate−1 coating systems. SEM cross-sectional analysis revealed that the polymer matrix in these coatings had fully degraded, with cracks extending through the coating and reaching towards the substrate. However, EIS measurements demonstrated that the praseodymium system still maintained impedance modulus values $|Z|_{0.01\ Hz}$ within the range of 10^7–$10^8\ \Omega\ cm^2$.

These results suggest that the anodized oxide layer, combined with the polymer embedded inside its pores, remained intact and continued to contribute to the corrosion protection. For reference, a fully intact anodized oxide layer without embedded polymer typically exhibits impedance modulus values $|Z|_{0.01\ Hz}$ in the range of 10^6–$10^7\ \Omega\ cm^2$.[38, 39] The higher impedance modulus values observed for the praseodymium system indicate that the polymer within the anodized oxide pores enhanced the overall corrosion resistance.

Mechanism 3: Enhanced pore resistance in the anodized oxide layer

The third proposed mechanism is based on observations from the chromate−1 system following outdoor

exposure. Despite complete failure of the polymer matrix inside the organic coating, the anodized oxide layer with its embedded polymer continued to provide effective corrosion protection, performing comparably to fully intact coating systems. EIS measurements consistently showed impedance modulus values $|Z|_{0.01\ Hz}$ exceeding $10^9\ \Omega\ cm^2$, even though SEM analysis revealed cracks in the organic coating extending towards the anodized aluminium substrate. These findings suggest that nanoscale cracks were effectively sealed by the formation of aluminium hydroxide, followed by the adsorption of chromate ions. This sealing likely restored pore resistance within the anodized oxide layer, accounting for the sustained electrochemical performance despite visible coating failure. Although similar processes have been proposed in earlier studies, the current findings provide further clarification that this self-healing mechanism occurs specifically within the anodized oxide layer.[26]

These insights highlight the complex interplay between inhibitor leaching, polymer degradation, and the integrity of the anodized oxide layer in maintaining long-term coating performance. These also underscore the risk of overlooking such long-term protective mechanisms in overly aggressive accelerated testing protocols.

Conclusions

This study demonstrates that immersion testing, outdoor exposure testing, and CSST do not adequately replicate the degradation mechanisms observed under actual in-service conditions. None of these test methods, as evaluated in this work, can be reliably used to predict the long-term in-service performance of structural aircraft coatings. The primary discrepancies arise from differences in degradation pathways, particularly those related to polymer breakdown and electrolyte exposure, which significantly influence the leaching behavior of corrosion inhibitors.

The findings highlight significant differences in how polymer matrices within coatings degrade across varying exposure environments. During outdoor exposure, polymer degradation is predominantly driven by UV-radiation, leading to oxidation and chain scissioning. By contrast, structural coatings in service are rarely, if ever, exposed to UV-radiation. CSST, on the other hand, predominantly induces polymer degradation through hydrolysis, whereas in-service conditions involve a combination of hydrolysis and thermo-oxidation.

In addition to polymer degradation, the solubility and release behavior of corrosion inhibitors play a critical role in the degradation of active protective coatings in the aerospace industry. The rate and extent of inhibitor leaching and the resulting degree of coating degradation are influenced by both the amount of electrolyte present as well as the exposure duration. Different exposure environments produce distinctly different impacts on coating degradation. For instance, under in-service conditions, inhibitors in chromate and lithium-based coatings exhibit only minimal leaching. However, the praseodymium system demonstrates relatively high inhibitor leaching, likely driven by the rapid dissolution of calcium sulphate in the primer. Under different exposure conditions, such as immersion, outdoor exposure or CSST, chromate-containing coatings experience significantly increased inhibitor leaching. This suggests that these testing methods subject coatings to more prolonged or intense electrolyte exposure as compared to in-service conditions. The structural coatings evaluated in this study are not designed to withstand such prolonged and unrealistic electrolyte contact. Instead, they are formulated in such way that these activate corrosion inhibition upon short-term wetting, accepting a reduction in barrier properties in order to provide localized corrosion protection at damaged sites. Therefore, extended exposure to electrolyte may not accurately reflect in-service performance. This highlights the importance of interpreting accelerated test results with caution, particularly for coating systems that rely on active inhibition mechanisms.

While both CSST and in-service testing reveal that coating degradation is primarily driven by the leaching of inhibitors, which is influenced by polymer degradation, they also reveal that inhibitor leaching does not typically extend to the substrate. Instead, coatings retain their barrier properties through intact polymer regions inside the coating in conjunction with an anodized oxide layer containing polymer embedded within its pores.

By contrast, outdoor exposure testing presents a unique case. Here, UV radiation severely damages the polymer matrix to the extent that cracks may propagate towards the substrate. Despite this, the polymer embedded inside the pores of the anodized oxide layer remains effective, providing a continued protection against corrosion. Notably, the chromate−1 system demonstrates exceptional performance under outdoor exposure conditions. Even in its damaged state, the coating retains protective properties comparable to those of an undamaged system. This extraordinary behavior is likely due to the formation of aluminium hydroxide, which, together with chromate adsorption, seals nanoscale cracks and transport pathways in the anodized oxide layer. This mechanism restores barrier properties and significantly enhances corrosion resistance.

Finally, this study underscores the value of ATR-FTIR analysis for detecting early stages of coating degradation, such as those observed during in-service conditions. ATR-FTIR proved particularly effective in identifying inhibitor leaching and initial polymer matrix degradation, demonstrating its potential as a powerful tool for understanding and monitoring coating degradation mechanisms. These findings highlight the utility of ATR-FTIR in providing detailed insights

into the early chemical changes within coatings, making it a critical tool for evaluating the chemical and functional integrity of coatings.

Acknowledgments The Logistic Centre Woensdrecht of the Royal Netherlands Air Force is gratefully acknowledged for both enabling this research and accommodating the research work.

Author contributions A.J. Cornet was contributed visualization, methodology, investigation, formal analysis, data curation, conceptualization, and writing–original draft. A.M. Homborg and J.M.C. Mol were involved in supervision and writing–review and editing. L. 't Hoen-Velterop was performed supervision, data curation, and writing–review and editing.

Data availability Data will be made available on request.

Conflict of interest The authors declare that they have no known competing financial interests or personal relationships that could have appeared to influence the work reported in this paper.

References

1. Mills, T, Prost-Domasky, S, Honeycutt, K, Brooks, C, ''Corrosion and the Threat to Aircraft Structural Integrity.'' In: *Corrosion Control in the Aerospace Industry*, pp. 35–66. Elsevier, Amsterdam. https://doi.org/10.1533/9781845695538.1.35 (2009)
2. Hughes, AE, Birbilis, N, Mol, JMC, Garcia, SJ, Xiaorong, Z, Thompson, GE, ''High Strength Al-Alloys: Microstructure, Corrosion and Principles of Protection.'' *Recent Trends Process. Degrad. Alumin. Alloys*, https://doi.org/10.5772/18766 (2011)
3. Andreatta, F, Fedrizzi, L, ''Corrosion Inhibitors.'' In: Hughes, A, Mol, J, Zheludkevich, M, Buchheit, R (eds) *Active Protective Coatings. Springer Series in Materials Science*, vol 233. Springer, Dordrecht (2016).https://doi.org/10.1007/978-94-017-7540-3_4
4. Hegedus, CR, Spadafora, SJ, Eng, AT, Pulley, DF, Hirst, DJ, ''Aerospace and Aircraft Coatings.'' In: Koleske, JV (ed.) *Paint and Coating Testing Manual: 15th. Edition of the Gardner-Sward Handbook*. https://doi.org/10.1520/mnl12239m (2012)
5. Jaya, A, Tiong, UH, Clark, G, ''The Interaction Between Corrosion Management and Structural Integrity of Aging Aircraft.'' *Fatigue Fract. Eng. Mater. Struct.*, https://doi.org/10.1111/j.1460-2695.2011.01562.x (2012)
6. Gharbi, O, Thomas, S, Smith, C, Birbilis, N, ''Chromate Replacement: What Does the Future Hold?'' *NPJ. Mater. Degrad.*, **2** 23–25. https://doi.org/10.1038/s41529-018-0034-5 (2018)
7. Cole, RA, ''Corrosion Prevention in the Aerospace Industries.'' *Anti-Corros. Methods Mater.*, **7** 320–324. https://doi.org/10.1108/eb019774 (1960)
8. Holmes, AL, Wise, SS, Wise, JP, ''Carcinogenicity of Hexavalent Chromium.'' *Indian J. Med. Res.*, **128** 353–372 (2008)
9. Azeez, NA, Dash, SS, Gummadi, SN, Deepa, VS, ''Nano-Remediation of Toxic Heavy Metal Contamination: Hexavalent Chromium [Cr(VI)].'' *Chemosphere*, **266** 129204. https://doi.org/10.1016/j.chemosphere.2020.129204 (2021)
10. Visser, P, Liu, Y, Terryn, H, Mol, JMC, ''Lithium Salts as Leachable Corrosion Inhibitors and Potential Replacement for Hexavalent Chromium in Organic Coatings for the Protection of Aluminum Alloys.'' *J. Coat. Technol. Res.*, **13** 557–566. https://doi.org/10.1007/s11998-016-9784-6 (2016)
11. Li, Z, Visser, P, Hughes, AE, Homborg, A, Gonzalez-Garcia, Y, Mol, A, ''Review of the State of Art of Li-Based Inhibitors and Coating Technology for the Corrosion Protection of Aluminium Alloys.'' *Surf. Coat. Technol.*, **478** 130441. https://doi.org/10.1016/J.SURFCOAT.2024.130441 (2024)
12. Frankel, GS, Buchheit, RG, Jaworowski, M, Swain, G, ''Scientific Understanding of Non-Chromated Corrosion Inhibitors Function SERDP Project WP-1620.'' (2013)
13. Bierwagen, G, Brown, R, Battocchi, D, Hayes, S, ''Active Metal-Based Corrosion Protective Coating Systems for Aircraft Requiring No-Chromate Pretreatment.'' *Prog. Org. Coat.*, **68** 48–61. https://doi.org/10.1016/j.porgcoat.2009.10.031 (2010)
14. Zhao, S, Birbilis, N, ''Searching for Chromate Replacements Using Natural Language Processing and Machine Learning Algorithms.'' *NPJ. Mater. Degrad.*, **7** 2. https://doi.org/10.1038/s41529-022-00319-0 (2023)
15. Twite, RL, Bierwagen, GP, ''Review of Alternatives to Chromate for Corrosion Protection of Aluminum Aerospace Alloys.'' *Prog. Org. Coat.*, **33** 91–100. https://doi.org/10.1016/S0300-9440(98)00015-0 (1998)
16. Grossman, GW, ''Correlation of Laboratory to Natural Weathering.'' *J. Coat. Technol.*, **49** (1977). https://www.q-lab.com/sites/default/files/Technical_Articles/Correlation-of-Laboratory-to-Natural-Weathering.pdf.
17. Knudsen, O, Skilbred, AWB, Løken, A, Daneshian, B, Höche, D, ''Correlations Between Standard Accelerated Tests for Protective Organic Coatings and Field Performance.'' *Mater. Today Commun.*, **31** 103729. https://doi.org/10.1016/j.mtcomm.2022.103729 (2022)
18. Zhang, T, Zhang, T, He, Y, Wang, Y, Bi, Y, ''Corrosion and Aging of Organic Aviation Coatings: A Review.'' *Chin. J. Aeronaut.*, **36** 1–35. https://doi.org/10.1016/j.cja.2022.12.003 (2023)

19. Peltier, F, Thierry, D, ''Development of a Reliable Accelerated Corrosion Test for Painted Aluminum Alloys Used in the Aerospace Industry.'' *Corros. Mater. Degrad.*, **5** 427–438. https://doi.org/10.3390/cmd5030019 (2024)
20. Lebozec, N, Blandin, N, Thierry, D, ''Accelerated Corrosion Tests in the Automotive Industry: A Comparison of the Performance Towards Cosmetic Corrosion.'' *Mater. Corros.*, **59** 889–894. https://doi.org/10.1002/maco.200804168 (2008)
21. Hao, P, Dun, Y, Gong, J, Li, S, Zhao, X, Tang, Y, Zuo, Y, ''Research Progress on Protective Performance Evaluation and Lifetime Prediction of Organic Coatings.'' *Anti-Corros. Methods Mater.*, https://doi.org/10.1108/ACMM-04-2024-2999 (2024)
22. Cornet, AJ, Homborg, AM, 't hoen-Velterop, L, Mol, JMC, ''Corrosion Protective Performance Evaluation of Structural Aircraft Coatings in Cyclic Salt Spray, Outdoor and In-Service Environments.'' *Eng. Fail Anal.*, **175** 109566. https://doi.org/10.1016/j.engfailanal.2025.109566 (2025)
23. Lebozec, N, Thierry, D, ''Influence of Climatic Factors in Cyclic Accelerated Corrosion Test Towards the Development of a Reliable and Repeatable Accelerated Corrosion Test for the Automotive Industry.'' *Mater. Corros.*, **61** 845–851. https://doi.org/10.1002/maco.200905497 (2010)
24. Baboian, R, *Corrosion Tests and Standards: Application and Interpretation-Second Edition*. (2005). https://doi.org/10.1520/mnl20-2nd-eb.
25. Cornet, AJ, Homborg, AM, Anusuyadevi, PR, 't Hoen-Velterop, L, Mol, JMC, ''Unravelling Corrosion Degradation of Aged Aircraft Components Protected by Chromate-Based Coatings.'' *Eng. Fail. Anal.*, **159** 108070. https://doi.org/10.1016/j.engfailanal.2024.1080704 (2024)
26. Cornet, AJ, Homborg, AM, 't Hoen-Velterop, L, Mol, JMC, ''Post-Service Analysis of the Degradation and Protective Mechanisms of Chromate-Based Structural Aircraft Coatings.'' *Prog. Org. Coat.*, **192** 108534. https://doi.org/10.1016/J.PORGCOAT.2024.108534 (2024)
27. Dante, J, ''Accelerated Dynamic Corrosion Test Method Development.'' Defense Technical Information Center, Alexandria, (2017). https://apps.dtic.mil/sti/citations/AD1053665.
28. Šoljić, I, Šoić, I, Kostelac, L, Martinez, S, ''AC Interference Impact on EIS Assessment of Organic Coatings Using Dummy Cells, Calibration Foils and Field Exposed Coated Samples.'' *Prog. Org. Coat.*, **165** 106767. https://doi.org/10.1016/j.porgcoat.2022.106767 (2022)
29. Galant, C, Fayolle, B, Kuntz, M, Verdu, J, ''Thermal and Radio-Oxidation of Epoxy Coatings.'' *Prog. Org. Coat.*, **69** 322–329. https://doi.org/10.1016/j.porgcoat.2010.07.005 (2010)
30. Djouani, F, Zahra, Y, Fayolle, B, Kuntz, M, Verdu, J, ''Degradation of Epoxy Coatings Under Gamma Irradiation.'' *Radiat. Phys. Chem.*, **82** 54–62. https://doi.org/10.1016/j.radphyschem.2012.09.008 (2013)
31. Ludwig, BW, Urban, MW, ''Quantitative Determination of Isocyanate Concentration in Crosslinked Polyurethane Coatings.'' *J. Coat. Technol.*, **68** 93–97 (1996)
32. Xu, A, Zhang, F, Jin, F, Zhang, R, Luo, B, Zhang, T, ''The Evaluation of Coating Performance by Analyzing the Intersection of Bode Plots.'' *Int. J. Electrochem. Sci.*, **9** 5116–5125. https://doi.org/10.1016/S1452-3981(23)08155-5 (2014)
33. Scully, JR, Hensley, ST, ''Lifetime Prediction for Organic Coatings on Steel and a Magnesium Alloy Using Electrochemical Impedance Methods.'' *Corrosion*, **50** 705–716. https://doi.org/10.5006/1.3293547 (1994)
34. Feng, Z, Frankel, GS, ''Evaluation of Coated Al Alloy Using the Breakpoint Frequency Method.'' *Electrochim. Acta*, **187** 605–615. https://doi.org/10.1016/j.electacta.2015.11.114 (2016)
35. Feng, Z, Frankel, GS, Matzdorf, CA, ''Quantification of Accelerated Corrosion Testing of Coated AA7075-T6.'' *J. Electrochem. Soc.*, **161** C42–C49. https://doi.org/10.1149/2.059401jes (2014)
36. Zheludkevich, ML, Shchukin, DG, Yasakau, KA, Möhwald, H, Ferreira, MGS, ''Anticorrosion Coatings with Self-Healing Effect Based on Nanocontainers Impregnated with Corrosion Inhibitor.'' *Chem. Mater.*, **19** 402–411. https://doi.org/10.1021/cm062066k (2007)
37. Zheludkevich, ML, Serra, R, Montemor, MF, Yasakau, KA, Salvado, IMM, Ferreira, MGS, ''Nanostructured Sol-Gel Coatings Doped with Cerium Nitrate as Pre-Treatments for AA2024-T3 Corrosion Protection Performance.'' *Electrochim. Acta*, **51** 208–217. https://doi.org/10.1016/j.electacta.2005.04.021 (2005)
38. Ding, Z, Smith, BA, Hebert, RR, Zhang, W, Jaworowski, MR, ''Morphology Perspective on Chromic Acid Anodizing Replacement by Thin Film Sulfuric Acid Anodizing.'' *Surf. Coat. Technol.*, **350** 31–39. https://doi.org/10.1016/j.surfcoat.2018.07.008 (2018)
39. Carangelo, A, Curioni, M, Acquesta, A, Monetta, T, Bellucci, F, ''Application of EIS to In Situ Characterization of Hydrothermal Sealing of Anodized Aluminum Alloys: Comparison Between Hexavalent Chromium-Based Sealing, Hot Water Sealing and Cerium-Based Sealing.'' *J. Electrochem. Soc.*, **163** C619. https://doi.org/10.1149/2.0231610jes (2016)
40. Hu, N, Dong, X, He, X, Browning, JF, Schaefer, DW, ''Effect of Sealing on the Morphology of Anodized Aluminum Oxide.'' *Corros. Sci.*, **97** 17–24. https://doi.org/10.1016/j.corsci.2015.03.021 (2015)
41. Hoseinpoor, M, Prošek, T, Babusiaux, L, Mallégol, J, ''Simplified Approach to Assess Water Uptake in Protective Organic Coatings by Parallel Plate Capacitor Method.'' *Mater. Today Commun.*, **26** 101858. https://doi.org/10.1016/j.mtcomm.2020.101858 (2021)
42. van Westing, EPM, Ferrari, GM, De Wit, JHW, ''The Determination of Coating Performance Using Electrochemical Impedance Spectroscopy.'' *Electrochim. Acta*, **39** 899–910. https://doi.org/10.1016/0013-4686(94)85104-2 (1994)
43. Van Der Wel, GK, Adan, OCG, ''Moisture in Organic Coatings—A Review.'' *Prog. Org. Coat.*, **37** 1–14. https://doi.org/10.1016/S0300-9440(99)00058-2 (1999)
44. Hughes, AE, Trinchi, A, Chen, FF, Yang, Y, Sellaiyan, S, Carr, J, Lee, PD, Thompson, GE, Xiao, TQ, ''Structure and Transport in Coatings from Multiscale Computed Tomography of Coatings—New Perspectives for Electrochemical Impedance Spectroscopy Modeling?'' *Electrochim. Acta*, **202** 243–252. https://doi.org/10.1016/j.electacta.2015.10.183 (2016)
45. Wouters, B, Jalilian, E, Claessens, R, Madelat, N, Hauffman, T, Van Assche, G, Terryn, H, Hubin, A, ''Monitoring Initial Contact of UV-Cured Organic Coatings with Aqueous Solutions Using Odd Random Phase Multisine Electrochemical Impedance Spectroscopy.'' *Corros. Sci.*, **190** 109713. https://doi.org/10.1016/j.corsci.2021.109713 (2021)
46. Zuo, Y, Pang, R, Li, W, Xiong, JP, Tang, YM, ''The Evaluation of Coating Performance by the Variations of Phase Angles in Middle and High Frequency Domains of

EIS.'' *Corros. Sci.*, **50** 3322–3328. https://doi.org/10.1016/j.corsci.2008.08.049 (2008)
47. Miszczyk, A, Darowicki, K, ''Water Uptake in Protective Organic Coatings and Its Reflection in Measured Coating Impedance.'' *Prog. Org. Coat.*, **124** 296–302. https://doi.org/10.1016/j.porgcoat.2018.03.002 (2018)
48. Yin, Y, Zhao, H, Prabhakar, M, Rohwerder, M, ''Organic Composite Coatings Containing Mesoporous Silica Particles: Degradation of the SiO_2 Leading to Self-Healing of the Delaminated Interface.'' *Corros. Sci.*, **200** 110252. https://doi.org/10.1016/j.corsci.2022.110252 (2022)
49. Santucci, RJ, Kannan, B, Abbott, W, Scully, JR, ''Scientific Investigation of the Corrosion Performance of Magnesium and Magnesium Oxide Primers on Al Alloy 2024–T351 in Field Exposures.'' *Corrosion*, **75** 440–456. https://doi.org/10.5006/2879 (2019)
50. Treu, BL, Pinc, W, Fahrenholtz, WG, O'Keefe, MJ, Morris, E, Albers, R, ''Characterization of Transport Processes in a Praseodymium-Containing Coating.'' *ECS Trans.*, **28** 229. https://doi.org/10.1149/1.3496434 (2010)
51. Lopez-Garrity, O, Frankel, GS, ''Corrosion Inhibition of Aluminum Alloy 2024–T3 by Praseodymium Chloride.'' *Corrosion*, **70** 928–941. https://doi.org/10.5006/1244 (2014)
52. Klomjit, P, Buchheit, RG, ''Cooperative and Synergistic Corrosion Inhibition of AA7075-T6 by Praseodymium and $CaSO_4$.'' *Corros. Rev.*, **38** 365–380. https://doi.org/10.1515/corrrev-2020-0032 (2020)
53. Lewis, OD, Critchlow, GW, Wilcox, GD, Dezeeuw, A, Sander, J, ''A Study of the Corrosion Resistance of a Waterborne Acrylic Coating Modified with Nano-Sized Titanium Dioxide.'' *Prog. Org. Coat.*, **73** 88–94. https://doi.org/10.1016/j.porgcoat.2011.09.004 (2012)
54. Cao, Y, Zheng, D, Dong, S, Zhang, F, Lin, J, Wang, C, Lin, C, ''A Composite Corrosion Inhibitor of MgAl layered Double Hydroxides Co-Intercalated with Hydroxide and Organic Anions for Carbon Steel in Simulated Carbonated Concrete Pore Solutions.'' *J. Electrochem. Soc.*, **166** C3106. https://doi.org/10.1149/2.0141911jes (2019)
55. Bouali, AC, Serdechnova, M, Blawert, C, Tedim, J, Ferreira, MGS, Zheludkevich, ML, ''Layered Double Hydroxides (LDHs) as Functional Materials for the Corrosion Protection of Aluminum Alloys: A Review.'' *Appl. Mater. Today*, **21** 100857. https://doi.org/10.1016/j.apmt.2020.100857 (2020)
56. Deyá, MC, Romagnoli, R, Romagnoli, R, Del Amo, B, ''The Influence of Zinc Oxide on the Anticorrosive Behaviour of Eco-Friendly Paints.'' *Corros. Rev.*, **22** 1–18. https://doi.org/10.1515/CORRREV.2004.22.1.1 (2004)
57. Alibakhshi, E, Ghasemi, E, Mahdavian, M, ''Corrosion Inhibition by Lithium Zinc Phosphate Pigment.'' *Corros. Sci.*, **77** 222–229. https://doi.org/10.1016/j.corsci.2013.08.005 (2013)
58. Cai, H, Li, X, Zhang, Y, Yang, C, Cui, S, Sheng, L, Xu, D, Fu, RKY, Tian, X, Chu, PK, Wu, Z, ''A High Corrosion-Resistant Waterborne Epoxy Resin Coating Improved by Addition of Multi-Interface Structured Zinc Phosphate Particles.'' *J. Mater. Res. Technol.*, **26** 7829–7844. https://doi.org/10.1016/j.jmrt.2023.09.109 (2023)
59. Bao, W, Deng, Z, Zhang, S, Ji, Z, Zhang, H, ''Next-Generation Composite Coating System: Nanocoating.'' *Front. Mater.*, **6** 72. https://doi.org/10.3389/fmats.2019.00072 (2019)
60. Vega, JM, Granizo, N, Simancas, J, de la Fuente, D, Díaz, I, Morcillo, M, ''Corrosion Inhibition of Aluminum by Organic Coatings Formulated with Calcium Exchange Silica Pigment.'' *J. Coat. Technol. Res.*, **10** 209–217. https://doi.org/10.1007/s11998-012-9440-8 (2013)
61. Vega, JM, Granizo, N, De La Fuente, D, Simancas, J, Morcillo, M, ''Corrosion Inhibition of Aluminum by Coatings Formulated with Al-Zn-Vanadate Hydrotalcite.'' *Prog. Org. Coat.*, **70** 213–219. https://doi.org/10.1016/j.porgcoat.2010.08.014 (2011)
62. Yang, XF, Vang, C, Tallman, DE, Bierwagen, GP, Croll, SG, Rohlik, S, ''Weathering Degradation of a Polyurethane Coating.'' *Polym. Degrad. Stab.*, **74** 341–351. https://doi.org/10.1016/S0141-3910(01)00166-5 (2001)
63. Gao, T, He, Z, Hihara, LH, Mehr, HS, Soucek, MD, ''Outdoor Exposure and Accelerated Weathering of Polyurethane/Polysiloxane Hybrid Coatings.'' *Prog. Org. Coat.*, **130** 45–57. https://doi.org/10.1016/j.porgcoat.2019.01.046 (2019)
64. Awaja, F, Pigram, PJ, ''Surface Molecular Characterisation of Different Epoxy Resin Composites Subjected to UV Accelerated Degradation Using XPS and ToF-SIMS.'' *Polym. Degrad. Stab.*, **94** 651–658. https://doi.org/10.1016/j.polymdegradstab.2009.01.001 (2009)
65. Kotnarowska, D, ''Influence of Ultraviolet Radiation and Aggressive Media on Epoxy Coating Degradation.'' *Prog. Org. Coat.*, **37** 149–159. https://doi.org/10.1016/S0300-9440(99)00070-3 (1999)
66. Asmatulu, R, Mahmud, GA, Hille, C, Misak, HE, ''Effects of UV Degradation on Surface Hydrophobicity, Crack, and Thickness of MWCNT-Based Nanocomposite Coatings.'' *Prog. Org. Coat.*, **72** 553–561. https://doi.org/10.1016/j.porgcoat.2011.06.015 (2011)
67. Larché, JF, Bussire, PO, Gardette, JL, ''How to Reveal Latent Degradation of Coatings Provoked by UV-Light.'' *Polym. Degrad. Stab.*, **95** 1810–1817. https://doi.org/10.1016/j.polymdegradstab.2010.05.005 (2010)
68. Croll, SG, ''Stress and Embrittlement in Organic Coatings During General Weathering Exposure: A Review.'' *Prog. Org. Coat.*, **172** 107085. https://doi.org/10.1016/j.porgcoat.2022.107085 (2022)
69. Andrew Chan, KL, Kazarian, SG, ''Attenuated Total Reflection Fourier-Transform Infrared (ATR-FTIR) Imaging of Tissues and Live Cells.'' *Chem. Soc. Rev.*, **45** 1850–1864. https://doi.org/10.1039/c5cs00515a (2016)
70. Morsch, S, Liu, Y, Lyon, SB, Gibbon, SR, Gabriele, B, Malanin, M, Eichhorn, KJ, ''Examining the Early Stages of Thermal Oxidative Degradation in Epoxy-Amine Resins.'' *Polym. Degrad. Stab.*, **176** 109147. https://doi.org/10.1016/j.polymdegradstab.2020.109147 (2020)
71. Xia, L, McCreery, RL, ''Chemistry of a Chromate Conversion Coating on Aluminum Alloy AA2024-T3 Probed by Vibrational Spectroscopy.'' *J. Electrochem. Soc.*, **145** 3083–3089. https://doi.org/10.1149/1.1838768 (1998)
72. Touina, A, Chernai, S, Mansour, B, Hadjar, H, Ouakouak, A, Hamdi, B, ''Characterization and Efficient Dye Discoloration of Algerian Diatomite from Ouled Djilali-Mostaganem.'' *SN Appl. Sci.*, **3** 476. https://doi.org/10.1007/s42452-021-04334-9 (2021)
73. Wu, Z, Li, S, Liu, M, Wang, Z, Liu, X, ''Liquid Oxygen Compatible Epoxy Resin: Modification and Characterization.'' *RSC Adv.*, **5** 11325–11333. https://doi.org/10.1039/c4ra14100h (2015)
74. Diebold, MP, ''Prediction of Paint Chalking Rates from Early Exposure Data.'' *J. Coat. Technol. Res.*, **20** 1179–1191. https://doi.org/10.1007/s11998-022-00727-6 (2023)
75. Socrates, G, *Infrared and Raman Characteristic Group Frequencies: Tables and Charts*, 3rd edn. John Wiley & Sons, Hoboken (2004)

76. Rivaton, A, Moreau, L, Gardette, J-L, ''Photo-Oxidation of Phenoxy Resins at Long and Short Wavelengths—II. Mechanisms of Formation of Photoproducts.'' *Polym. Degrad. Stab.*, **58** 333–339. https://doi.org/10.1016/S0141-3910(97)00088-8 (1997)
77. Delannoy, R, Tognetti, V, Richaud, E, ''Experimental and Theoretical Insights on the Thermal Oxidation of Epoxy-Amine Networks.'' *Polym. Degrad. Stab.*, **206** 110188. https://doi.org/10.1016/j.polymdegradstab.2022.110188 (2022)
78. Meiser, A, Willstrand, K, Possart, W, ''Influence of Composition, Humidity, and Temperature on Chemical Aging in Epoxies: A Local Study of the Interphase with Air.'' *J. Adhes.*, **86** 222–243. https://doi.org/10.1080/00218460903418352 (2010)
79. Chen, K, Zhao, X, Zhang, F, Wu, X, Huang, W, Liu, W, Wang, X, ''Influence of Gamma Irradiation on the Molecular Dynamics and Mechanical Properties of Epoxy Resin.'' *Polym. Degrad. Stab.*, **168** 108940. https://doi.org/10.1016/j.polymdegradstab.2019.108940 (2019)
80. Hoffmann, MM, Darab, JG, Fulton, JL, ''An Infrared and X-ray Absorption Study of the Equilibria and Structures of Chromate, Bichromate, and Dichromate in Ambient Aqueous Solutions.'' *J. Phys. Chem. A*, **105** 1772–1782. https://doi.org/10.1021/jp0027041 (2001)
81. Hedberg, YS, Wei, Z, McCarrick, S, Romanovski, V, Theodore, J, Westin, EM, Wagner, R, Persson, KA, Karlsson, HL, Odnevall Wallinder, I, ''Welding Fume Nanoparticles from Solid and Flux-Cored Wires: Solubility, Toxicity, and Role of Fluorides.'' *J. Hazard. Mater.*, **413** 125273. https://doi.org/10.1016/j.jhazmat.2021.125273 (2021)
82. Vats, V, Melton, G, Islam, M, Krishnan, VV, ''FTIR Spectroscopy as a Convenient Tool for Detection and Identification of Airborne Cr(VI) Compounds Arising from Arc Welding Fumes.'' *J. Hazard. Mater.*, **448** 130862. https://doi.org/10.1016/j.jhazmat.2023.130862 (2023)
83. Muller, O, White, WB, Roy, R, ''Infrared Spectra of the Chromates of Magnesium, Nickel and Cadmium.'' *Spectrochim. Acta A*, **25** 1491–1499. https://doi.org/10.1016/0584-8539(69)80133-9 (1969)
84. Nga, NK, Thuy Chau, NT, Viet, PH, ''Preparation and Characterization of a Chitosan/MgO Composite for the Effective Removal of Reactive Blue 19 Dye from Aqueous Solution.'' *J. Sci.: Adv. Mater. Dev.*, **5** 65–72. https://doi.org/10.1016/j.jsamd.2020.01.009 (2020)
85. Zahir, MH, Rahman, MM, Irshad, K, Rahman, MM, ''Shape-Stabilized Phase Change Materials for Solar Energy Storage: MgO and $Mg(OH)_2$ Mixed with Polyethylene Glycol.'' *Nanomater.*, **9** 1773. https://doi.org/10.3390/nano9121773 (2019)
86. Santucci, RJ, Scully, JR, ''Mechanistic Framework for Understanding pH-Induced Electrode Potential Control of AA2024-T351 by Protective Mg-Based Pigmented Coatings.'' *J. Electrochem. Soc.*, **167** 131514. https://doi.org/10.1149/1945-7111/abbd74 (2020)
87. Melo, HP, Cruz, AJ, Candeias, A, Mirão, J, Cardoso, AM, Oliveira, MJ, Valadas, S, ''Problems of Analysis by FTIR of Calcium Sulphate-Based Preparatory Layers: The Case of a Group of 16th-Century Portuguese Paintings.'' *Archaeometry*, **56** 513–526. https://doi.org/10.1111/arcm.12026 (2014)
88. Ennaciri, Y, Bettach, M, Cherrat, A, Zegzouti, A, ''Conversion of Phosphogypsum to Sodium Sulfate and Calcium Carbonate in Aqueous Solution.'' *J. Mater. Environ. Sci.,* **7** (2016)
89. Kamaraj, C, Lakshmi, S, Rose, C, Muralidharan, C, ''Wet Blue Fiber and Lime from Leather Industry Solid Waste as Stabilizing Additive and Filler in Design of Stone Matrix Asphalt.'' *Asian J. Res. Soc. Sci. Humanit.*, **7** 240. https://doi.org/10.5958/2249-7315.2017.00547.0 (2017)
90. Kadam, SS, Mesbah, A, van der Windt, E, Kramer, HJM, ''Rapid Online Calibration for ATR-FTIR Spectroscopy During Batch Crystallization of Ammonium Sulphate in a Semi-Industrial Scale Crystallizer.'' *Chem. Eng. Res. Des.*, **89** 995–1005. https://doi.org/10.1016/j.cherd.2010.11.013 (2011)
91. Verma, SK, Deb, MK, ''Direct and Rapid Determination of Sulphate in Environmental Samples with Diffuse Reflectance Fourier Transform Infrared Spectroscopy Using KBr Substrate.'' *Talanta*, **71** 1546–1552. https://doi.org/10.1016/j.talanta.2006.07.056 (2007)
92. Ravi Teja, V, Sreenivasulu, M, Chavan, VK, ''Praseodymium Ion-Doped Boro Lithium Glass Material for Optical Applications: W-LED.'' *J. Mater. Sci.: Mater. Electron.*, **35** 166. https://doi.org/10.1007/s10854-023-11897-3 (2024)
93. Balachandran, S, Karthikeyan, R, Selvakumar, K, Swaminathan, M, ''Photo-Electrocatalytic Activity of Praseodymium Oxide Modified Titania Nanorods.'' *Int. J. Environ. Anal. Chem.*, https://doi.org/10.1080/03067319.2020.1790541 (2020)
94. Kang, JG, Min, BK, Sohn, Y, ''Physicochemical Properties of Praseodymium Hydroxide and Oxide Nanorods.'' *J. Alloys Compd.*, **619** 165–171. https://doi.org/10.1016/j.jallcom.2014.09.059 (2015)
95. Treu, BL, Fahrenholtz, W, O'Keefe, M, Morris, E, Albers, R, ''Effect of Phase on the Electrochemical and Morphological Properties of Praseodymium-Based Coatings.'' *ECS Trans.*, **33** 53. https://doi.org/10.1149/1.3577753 (2011)
96. Klomjit, P, Buchheit, RG, ''Localized Corrosion Inhibition of AA7075-T6 by Calcium Sulfate.'' *Corrosion*, **72** 486–499. https://doi.org/10.5006/1892 (2016)
97. Klomjit, P, Buchheit, RG, ''Characterization of Inhibitor Storage and Release From Commercial Primers.'' *Prog. Org. Coat.*, **114** 68–77. https://doi.org/10.1016/J.PORGCOAT.2017.10.005 (2018)
98. Weber, G, Sciora, E, Guichard, J, Bouyer, F, Bezverkhyy, I, Marcos Salazar, J, Dirand, C, Bernard, F, Lecoq, H, Besnard, R, Bellat, JP, ''Investigation of Hydrolysis of Lithium Oxide by Thermogravimetry, Calorimetry and In Situ FTIR Spectroscopy.'' *J. Therm. Anal. Calorim.*, **132** 1055–1064. https://doi.org/10.1007/s10973-017-6943-7 (2018)
99. Rajabimashhadi, Z, Naghizadeh, R, Zolriasatein, A, Bagheri, S, Mele, C, Esposito Corcione, C, ''Hydrophobic, Mechanical, and Physical Properties of Polyurethane Nanocomposite: Synergistic Impact of $Mg(OH)_2$ and SiO_2.'' *Polymers (Basel)*, **15** 1916. https://doi.org/10.3390/polym15081916 (2023)
100. Rabbani, S, Bakhshandeh, E, Jafari, R, Momen, G, ''Superhydrophobic and Icephobic Polyurethane Coatings: Fundamentals, Progress, Challenges and Opportunities.'' *Prog. Org. Coat.*, **165** 106715. https://doi.org/10.1016/j.porgcoat.2022.106715 (2022)
101. Amrollahi, M, Sadeghi, GMM, ''Assessment of Adhesion and Surface Properties of Polyurethane Coatings Based on Non-Polar and Hydrophobic Soft Segment.'' *Prog. Org. Coat.*, **93** 23–33. https://doi.org/10.1016/j.porgcoat.2015.12.001 (2016)
102. Liu, FC, Hao, YS, Wang, ZY, Shi, HW, Han, EH, Ke, W, ''Flaking and Degradation of Polyurethane Coatings After 2 Years of Outdoor Exposure in Lhasa.'' *Chin. Sci. Bull.*, **55** 650–655. https://doi.org/10.1007/s11434-009-0269-1 (2010)
103. Merlatti, C, Perrin, FX, Aragon, E, Margaillan, A, ''Natural and Artificial Weathering Characteristics of Stabilized Acrylic-Urethane Paints.'' *Polym. Degrad. Stab.*, **93** 896–

903. https://doi.org/10.1016/j.polymdegradstab.2008.02.008 (2008)
104. Ben Bechir, M, Ben Rhaiem, A, ''The Lithium-Ion Battery: Study of Alternative Current Conduction Mechanisms on the Li_3PO_4 - Based Solid Electrolyte.'' *Phys. E Low. Dimens. Syst. Nanostruct.*, **130** 114686. https://doi.org/10.1016/j.physe.2021.114686 (2021)
105. Olgiati, M, Denissen, PJ, Garcia, SJ, ''When All Intermetallics Dealloy in AA2024-T3: Quantifying Early Stage Intermetallic Corrosion Kinetics Under Immersion.'' *Corros. Sci.*, **192** 109836. https://doi.org/10.1016/j.corsci.2021.109836 (2021)
106. Coelho, LB, Lukaczynska-Anderson, M, Clerick, S, Buytaert, G, Lievens, S, Terryn, HA, ''Corrosion Inhibition of AA6060 by Silicate and Phosphate in Automotive Organic Additive Technology Coolants.'' *Corros. Sci.*, **199** 110188. https://doi.org/10.1016/j.corsci.2022.110188 (2022)
107. Tanks, JD, Kubouchi, M, Arao, Y, ''Influence of Network Structure on the Degradation of Poly(Ether)Amine-Cured Epoxy Resins by Inorganic Acid.'' *Polym. Degrad. Stab.*, **157** 153–159. https://doi.org/10.1016/j.polymdegradstab.2018.10.011 (2018)
108. Shen, M, Almallahi, R, Rizvi, Z, Gonzalez-Martinez, E, Yang, G, Robertson, ML, ''Accelerated Hydrolytic Degradation of Ester-Containing Biobased Epoxy Resins.'' *Polym. Chem.*, **10** 3217–3229. https://doi.org/10.1039/c9py00240e (2019)
109. Oliveira, MS, da Luz, FS, Pereira, AC, Costa, UO, Bezerra, WBA, da Cunha, JdosSC, Lopera, HAC, Monteiro, SN, ''Water Immersion Aging of Epoxy Resin and Fique Fabric Composites: Dynamic–Mechanical and Morphological Analysis.'' *Polymers (Basel)*, **14** 3650. https://doi.org/10.3390/polym14173650 (2022)
110. Pickett, JE, Coyle, DJ, ''Hydrolysis Kinetics of Condensation Polymers Under Humidity Aging Conditions.'' *Polym. Degrad. Stab.*, **98** 1311–1320. https://doi.org/10.1016/j.polymdegradstab.2013.04.001 (2013)
111. Moniruzzaman, M, Kobayashi, T, Sasaki, T, ''Solubility of Mixed Lanthanide Hydroxide and Oxide Solid Solutions.'' *J. Nucl. Fuel Cycle Waste Technol.*, **19** 353–366. https://doi.org/10.7733/jnfcwt.2021.19.3.353 (2021)
112. Bhargava, S, Kubota, M, Lewis, RD, Advani, SG, Prasad, AK, Deitzel, JM, ''Ultraviolet, Water, and Thermal Aging Studies of a Waterborne Polyurethane Elastomer-Based High Reflectivity Coating.'' *Prog. Org. Coat.*,. https://doi.org/10.1016/j.porgcoat.2014.11.005 (2015)
113. Frankel, GS, Clayton, CR, Granata, RD, Kendig, M, Isaacs, HS, McCreery, RL, Stratmann, M, ''Mechanism of Al Alloy Corrosion and the Role of Chromate Inhibitors.'' https://apps.dtic.mil/sti/tr/pdf/ADA399114.pdf (2001)